© 2014. Published by The Company of Biologists Ltd | The Journal of Experimental Biology (2014) 217, 1983-1992 doi:10.1242/jeb.096362

RESEARCH ARTICLE

In vivo cranial bone strain and bite force in the agamid lizard *Uromastyx geyri*

Laura B. Porro[1,2,‡], Callum F. Ross[1], Jose Iriarte-Diaz[1,*], James C. O'Reilly[1], Susan E. Evans[3] and Michael J. Fagan[4]

ABSTRACT

In vivo bone strain data are the most direct evidence of deformation and strain regimes in the vertebrate cranium during feeding and can provide important insights into skull morphology. Strain data have been collected during feeding across a wide range of mammals; in contrast, *in vivo* cranial bone strain data have been collected from few sauropsid taxa. Here we present bone strain data recorded from the jugal of the herbivorous agamid lizard *Uromastyx geyri* along with simultaneously recorded bite force. Principal and shear strain magnitudes in *Uromastyx geyri* were lower than cranial bone strains recorded in *Alligator mississippiensis*, but higher than those reported from herbivorous mammals. Our results suggest that variations in principal strain orientations in the facial skeleton are largely due to differences in feeding behavior and bite location, whereas food type has little impact on strain orientations. Furthermore, mean principal strain orientations differ between male and female *Uromastyx* during feeding, potentially because of sexual dimorphism in skull morphology.

KEY WORDS: Feeding, Skull, Biomechanics, Squamates

INTRODUCTION

In vivo bone strains provide direct evidence of strain regimes (*sensu* Ross et al., 2011) in skeletal structures during function. Data collected from the skull during feeding reveal strain patterns produced by internal and external loads; specifically, muscle forces and reaction forces at the jaw joints and teeth. Strain orientations are used to reveal the load transfer path and infer the deformation regime of the skull, while variations in strain magnitude highlight areas that are more or less subjected to deformation and thus adapted to resist feeding forces. Comparing strain orientations, magnitudes and distributions in the skulls of different taxa reveals aspects of cranial architecture adapted to particular diets, feeding behaviors or factors other than feeding.

In vivo bone strain data have been recorded from the crania of primates (Hylander and Johnson, 1997; Hylander et al., 1987; Ross, 2001; Ross and Hylander, 1996; Ross et al., 2011), sheep (Thomason et al., 2001), pigs (Herring and Teng, 2000) and hyraxes (Lieberman et al., 2004). These studies reveal significant variation in bone strain magnitudes across the skull during feeding, with higher strains in the facial skeleton and mandible than in the braincase or circumorbital region (Hylander et al., 1991a; Hylander et al., 1991b; Ravosa et al., 2000a; Ravosa et al., 2000b; Ross and Hylander, 1996; Ross and Metzger, 2004). Such highly strained areas of the skull are likely to be better optimized to resist loads generated during feeding, where optimality is defined as maximum strength for minimum material. In contrast, areas of the skull exhibiting low strain magnitudes during feeding instead function to protect the brain or eyes (Heesy, 2005; Hylander and Johnson, 1992; Hylander and Johnson, 1997; Ravosa et al., 2000a; Ross, 1995a), serve as areas for muscle attachment (Ross, 1995b) or provide a rigid framework to keep respiratory pathways open (Ross, 1995b; Ross, 2001; Ross and Metzger, 2004).

In vivo bone strain data have been recorded from the skulls of few non-mammalian taxa. Strain recorded from the cranium (Metzger et al., 2005) and lower jaw (Porro et al., 2013) of *Alligator mississippiensis* reveal heterogeneity in strain magnitudes in the skull. On average, maximum principal strain (ε_1) magnitudes in the *A. mississippiensis* skull during feeding are high compared with those recorded in mammals: all gage sites on the *A. mississippiensis* cranium experienced ε_1 strains over 1000 microstrain (με, which are equal to 1×10^{-6} inches inch^{-1} or mm mm^{-1}) during at least one loading condition (Metzger et al., 2005), while the grand mean across all gage sites in the lower jaw was over 900 με (Porro et al., 2013). ε_1 strains measured in the frontal bone of *Varanus exanthematicus* during feeding ranged from 100 to 600 με, although values as high as 2000 με were recorded (Smith and Hylander, 1985). In contrast, many areas of mammalian crania never experience strain magnitudes over 100 με. Results from these sauropsids suggest that their cranial morphology may be better optimized to resist feeding forces than mammalian crania, possibly because their relatively smaller brains are housed within the bony framework of the skull (Curtis et al., 2011; Curtis et al., 2013).

Lepidosaur skulls exhibit diverse feeding adaptations including clade- and diet-specific differences in skull and tooth morphology, and cranial kinetic potential (Herrel et al., 2001a; Herrel et al., 2001b; Herrel et al., 2004; Herrel et al., 2007; Metzger, 2002; Metzger and Herrel, 2005; Rieppel and Labhardt, 1979; Robinson, 1976; Schwenk, 2000; Stayton, 2005; Stayton, 2006). *Uromastyx* is a genus of agamid lizards found in northern Africa, the Middle East and south-central Asia. It is primarily herbivorous and, over the past three decades, has become a model for analysis of skull form and function. *Uromastyx* is characterized by specialized skull morphology and an acrodont dentition in which the teeth are fused to the jaw bones. Teeth are not replaced in adults, resulting in the

[1]Department of Organismal Biology and Anatomy, University of Chicago, 1027 East 57th Street, Chicago, IL 60637, USA. [2]School of Earth Sciences, University of Bristol, Wills Memorial Building, Queen's Road, Bristol BS8 1RJ, UK. [3]Research Department of Cell and Developmental Biology, University College London, Gower Street, London WCIE 6BT, UK. [4]School of Engineering, University of Hull, Cottingham Road, Hull HU6 7RX, UK.
*Present address: Department of Oral Biology, University of Illinois at Chicago, 801 S. Paulina St., Chicago, IL 60612, USA.

‡Author for correspondence (laura.porro@bristol.ac.uk)

Received 29 August 2013; Accepted 8 February 2014

development of extensive wear facets (Robinson, 1976; Throckmorton, 1979). Unlike most sauropsids, *Uromastyx* engages in cyclic intra-oral food processing (i.e. chewing), resulting in food being broken into smaller pieces. Chewing is distinct from mastication, a term reserved for mammals, as the latter involves transverse movements of the teeth during the power stroke and precise tooth–tooth occlusion (Throckmorton 1976; Throckmorton, 1980; Ross et al., 2007; Crompton, 1989). Chewing cycles in *Uromastyx* are longer, slower and less rhythmic than in mammals (Throckmorton, 1980; Ross et al., 2007), involve retraction of the jaw during closure (Throckmorton, 1976), and possible rotation of the lower jaw about its long axis as the teeth come into occlusion (Throckmorton, 1974; Throckmorton, 1980). The cranium of *Uromastyx* exhibits streptostyly (antero-posterior rotation of the quadrate against the squamosal) (Throckmorton, 1976; Herrel and De Vree, 1999). Previous *in vivo* experimental work on *Uromastyx* has included descriptions of lower jaw, tongue and streptostylic movements during feeding (Throckmorton, 1976; Throckmorton, 1980; Herrel and De Vree, 1999), electromyographic analysis of jaw and hyolingual muscle activity (Throckmorton, 1978; Throckmorton, 1980; Herrel and De Vree, 2009), and measurements of bite force (Herrel and De Vree, 2009).

Additionally, *Uromastyx* has been modeled using both multibody dynamics analysis (MDA), to simulate rigid-body motion under feeding loads, and finite element analysis (FEA), to understand the internal mechanical behavior of the cranium during feeding (Moazen et al., 2008a; Moazen et al., 2008b; Moazen et al., 2009a; Moazen et al., 2009b). Advantages of these methods compared with experimental techniques include measuring strain throughout the entire structure and predicting variables that are difficult or impossible to measure *in vivo* (such as joint reaction forces). However, model accuracy is dependent on input parameters used in their construction (Gröning et al., 2013). MDA modeling requires kinematic data to drive feeding simulations, while simultaneously recorded electromyographic and bite force data can be used to test model accuracy. Similarly, the accuracy of FEA is improved with detailed knowledge of muscle architecture and activity and bone material properties, while bone strains predicted by FEA can be validated against experimental strain data. Validation studies comparing predictions from finite element model (FEM) skulls with *in vivo* data have been largely confined to mammals (Verrue et al., 2001; Ross et al., 2005; Ross et al., 2011; Strait et al., 2005), with the cranium and lower jaw of *Alligator* representing the only non-mammalian FEMs for which *in vivo* validation studies have been carried out (Metzger et al., 2005; Porro et al., 2013). Until *Uromastyx* MDA and FEA results are validated against experimental data, it is unclear how well model predictions reflect reality.

In this paper, we present simultaneous bone strains and bite forces obtained during feeding in *Uromastyx geyri* Müller 1922; these data represent the first measurements of *in vivo* cranial bone strain obtained for an herbivorous sauropsid. The aims of this study are to: (1) document *in vivo* bone strains in the *U. geyri* cranium during feeding; (2) examine variations in strain magnitudes, principal strain orientations and ratios among individuals and with changes in bite location, food type and feeding behavior; (3) compare strain magnitudes in *U. geyri* with those obtained from other sauropsids and mammals; and (4) examine the relationship between bite force and strain magnitude.

RESULTS

In some cases, gages failed during experiments or movement artifacts rendered data unusable. As a result, different amounts of data are available for each animal and for individual gage sites. The individual Uro1 yielded the largest data set, followed by Uro5 and Uro7.

Observations of feeding behavior

Feeding sequences (defined as the series of behaviors during the ingestion of a single food item) were composed of individual cycles representing eight distinct feeding behaviors. Eighty-nine feeding sequences were recorded from the three subjects. The number of cycles per sequence ranged from two to 40 cycles, with a mean of 14 cycles per sequence; these results are similar to those reported by Throckmorton (Throckmorton, 1980) in *U. aegyptius* and Herrel and De Vree (Herrel and De Vree, 1999) in *U. acanthinurus*. Data were recorded during 39 transducer bites in Uro5. In total, data were collected for 1364 individual cycles.

A typical feeding sequence began with tongue flicks, characterized by low gape angles and rapid protrusion and retraction of the tongue; the tip of the tongue either contacted the food directly or the floor in front of the food [referred to as ‘tasting’ by Throckmorton (Throckmorton, 1980); specified as tongue touches by Herrel et al. (Herrel et al., 1998), in which kinematics and electromyography are also described]. Food was acquired during capture cycles: the animal approached the food, the jaws were opened slightly and the tongue protruded with its tip curled ventrally so that the dorsum of the tongue contacted the food (Throckmorton, 1980; Herrel and De Vree, 1999). The tongue, with the food adhered to it, was pulled back into the mouth as the jaws opened quickly and widely and the food was grasped in the anterior jaws. The animals then exhibited a variable number of manipulation cycles: these were characterized by the jaws opening rapidly to a wide gape, sharp lateral and ventral movements of the head as well as rolling of the head about its long axis, followed by rapid jaw closure. The purpose of these manipulation cycles is to shift the food from the front of the jaws to a posterior region of the tooth row more suitable for reduction. Manipulation cycles were followed by chewing: compared with manipulation cycles, chewing involved little or no movement of the head (which was usually held with the palate horizontal), low gape angles, and slower jaw opening and closure. Chewing resulted in the food being broken or folded into smaller pieces. The tongue was used to position food during both manipulation and chewing cycles. Chewing cycles were often interspersed with manipulation cycles as the animal finished reducing a portion of the food (especially larger leaves) and moved new portions to a more posterior position along the tooth row. Swallowing cycles were followed by licking cycles [referred to as ‘cleaning’ by Throckmorton (Throckmorton, 1980)], in which the animal opened the jaws slightly, the tongue protruded just beyond the anterior margins of the jaws and then retracted, and the jaws closed.

Two additional feeding behaviors were documented. Crushing occurred when the animals ate Mazuri pellets. The animal shifted the pellet to a posterior position of the tooth row (using manipulation cycles), then closed the jaws slowly and powerfully until the pellet failed suddenly, fracturing into several pieces within and outside of the mouth. In rare instances, the animal would brace the lower jaw against the ground during crushing, presumably to allow neck flexor muscles to contribute to the bite force. Crushing described in other agamids involves numerous cyclic movements (Herrel et al., 1997); *U. geyri* exhibited only one or two crushing cycles during a feeding sequence. Crushing cycles were followed immediately by chewing or swallowing cycles. Tearing resulted when the animal held a food item (usually a leaf) down with a foreleg while using movements of the head and neck to tear pieces from it. This behavior was rare (only five instances were recorded).

The Journal of Experimental Biology

Food was always ingested at the front of the jaws and shifted to a posterior position for reduction. In some instances, particularly when feeding on Mazuri pellets, animals shifted food to one side of the head for processing; in these cases, working and balancing sides were clear. In most instances, the food item protruded from both sides of the mouth during reduction. Thus, bite location could be clearly assigned to only 32% of all cycles recorded.

Principal strain magnitudes and ratios

Mean and peak principal strain magnitudes were highest in Uro1, followed by Uro7 and Uro5 (supplementary material Tables S1–S3); the highest recorded principal strain (Uro1) was −1936 με. Working-side bites typically produced higher mean maximum (ε_1) and minimum (ε_2) principal strains than balancing-side or frontal bites (Fig. 1). Frontal bites produced the lowest mean strains in Uro1 and Uro7; balancing-side bites produced the lowest mean strains in Uro5. Feeding on greens produced higher mean ε_1 and ε_2 strains in all three individuals, although the highest peak principal strains occurred when feeding on Mazuri pellets. Transducer biting produced the highest mean principal strains in Uro5. In all three animals, tongue flicks, captures, swallows and licks produced low strains; the highest strains were generated during manipulation, crushing and chewing cycles.

Two-way mixed-model ANOVA (supplementary material Table S10) revealed significant effects of feeding behavior on ε_1 and ε_2 magnitudes at all analyzed gage sites. Individual differences account for significant variation in strain magnitude in the left jugal (48%) but not the right jugal (12%). Additionally, there were significant interaction effects between food type and behavior on ε_2 magnitude (both sides) and ε_1 magnitude (left jugal only). Food type typically did not significantly impact ε_1 magnitude. *Post hoc* comparisons revealed that, at both gage sites, mean ε_1 magnitudes elicited during manipulation and chewing were different from each other, and from those elicited during swallowing and licking; mean ε_1 strain magnitudes during the latter two behaviors did not differ from each other. This was true for mean ε_2 magnitudes, except that swallowing and licking differed from each other in the right gage. ANOVA testing for differences in principal strain magnitudes due to bite location revealed a significant effect of bite point at both gage sites (supplementary material Table S11).

The grand mean of maximum to minimum principal strain ratios ($|\varepsilon_1/\varepsilon_2|$) for all *in vivo* experiments was 1.76; within-gage means for all individuals was always >1, suggesting that tension is the predominant loading regime experienced by the *U. geyri* jugal during feeding (supplementary material Tables S1–S3). This is consistent with FEA of the *Uromastyx hardwickii* skull, which predicted that the ventral jugal is an area of high tensile strain during biting (Moazen et al., 2008a). The $\varepsilon_1/\varepsilon_2$ ratio was higher during frontal (Uro7, left gage of Uro5) or balancing-side bites (Uro1, right gage of Uro5) than during working-side bites; this is consistent with the expectation that anterior bites would load the jugal in tension while working-side bites would load the jugal in compression. Mean $\varepsilon_1/\varepsilon_2$ was >1 during transducer biting in Uro5, suggesting that tension was the predominant loading regime in the jugal; this is consistent with frontal bites placing the jugal in tension. Patterns in $\varepsilon_1/\varepsilon_2$ ratios were most consistent when data were sorted by feeding behaviors: tongue flicks, chews, licks and swallows nearly always produced $\varepsilon_1/\varepsilon_2$ ratios >1, indicating that the jugals experienced tension during these behaviors. Crushing always produced $\varepsilon_1/\varepsilon_2$ ratios <1, indicating that this behavior (which occurred in the posterior portion of the tooth row) compressed the jugals (supplementary material Tables S1–S3). $\varepsilon_1/\varepsilon_2$ ratios were highly variable during capture, manipulation and tearing cycles, most likely because of large and unpredictable head movements. Two-way ANOVA revealed significant effects of feeding behavior, as well as the interaction between food type and behavior, on $\varepsilon_1/\varepsilon_2$ ratios at both gage sites (supplementary material Table S10). ANOVA testing revealed significant differences in principal strain ratios due to bite location at both gage sites (supplementary material Table S11).

Principal strain orientations

Vector plots of strain orientation (Fig. 2) reveal two distinct strain regimes in the jugals of *U. geyri* during feeding, suggesting two separate loading regimes. For the three individuals, strain orientations were sorted by bite location, food type and feeding behavior to attempt to separate these loading regimes.

Mean ε_1 orientation for all cycles in Uro1 was anteriorly directed in the right jugal and anterodorsally directed in the left jugal (supplementary material Table S2). On both sides, ε_1 vectors during working-side bites were rotated counterclockwise compared with strains generated during frontal bites (supplementary material Table S2). The two strain regimes are most apparent when data are sorted by feeding behavior: for both right and left gages in Uro1, mean ε_1 was generally directed anteroventrally during tongue flick, capture, lick and swallow cycles, and anterodorsally during manipulation, crushing and chewing (Fig. 2; supplementary material Table S2).

Mean vector length and concentration reveal that ε_1 strain orientations were more concentrated during posterior bites than during frontal bites in Uro1 (supplementary material Table S4); additionally, ε_1 strain orientations were most concentrated during crushing and licking cycles and most variable during capture cycles (supplementary material Table S6). Mardia–Watson–Wheeler tests demonstrate that ε_1 orientations were significantly different with changes in bite location, food type and feeding behavior (supplementary material Tables S7–S9).

In Uro5, mean ε_1 orientation for all cycles was anteriorly directed in the left jugal, and changes in ε_1 orientations with bite location, food type and feeding behavior resembled trends observed in Uro1 (Fig. 2; supplementary material Table S1). In contrast, mean ε_1 in the right jugal of Uro5 was anterodorsally directed and showed little variability with changes in bite location or food type. Mardia–Watson–Wheeler tests demonstrate that ε_1 orientations were significantly different with changes in bite point (supplementary material Table S7) and food type (supplementary material Table S8) in the right jugal of Uro5.

Unlike Uro1 and Uro5, mean ε_1 orientation in both jugals of Uro7 was anteroventrally directed (supplementary material Table S3). However, changes in ε_1 orientation with bite location, food type and feeding behavior were asymmetric between the right and left jugals. In the right jugal, ε_1 was rotated clockwise during posterior bites compared with frontal biting; the opposite pattern was observed in the left jugal (supplementary material Table S3). In the right jugal of Uro7, ε_1 was rotated counterclockwise during tongue flick, capture and chewing cycles compared with other feeding behaviors; these behaviors caused clockwise rotation of ε_1 in the left jugal (supplementary material Table S3).

As in Uro1, mean vector length and concentration reveal that ε_1 strain orientations were less variable during posterior bites than during frontal bites on both sides of Uro7 (supplementary material Table S4). Right and left ε_1 strain orientations were most concentrated during crushing in Uro7 (supplementary material Table S6). Mardia–Watson–Wheeler tests demonstrate that ε_1 orientations were significantly different during feeding on different

The Journal of Experimental Biology (2014) doi:10.1242/jeb.096362

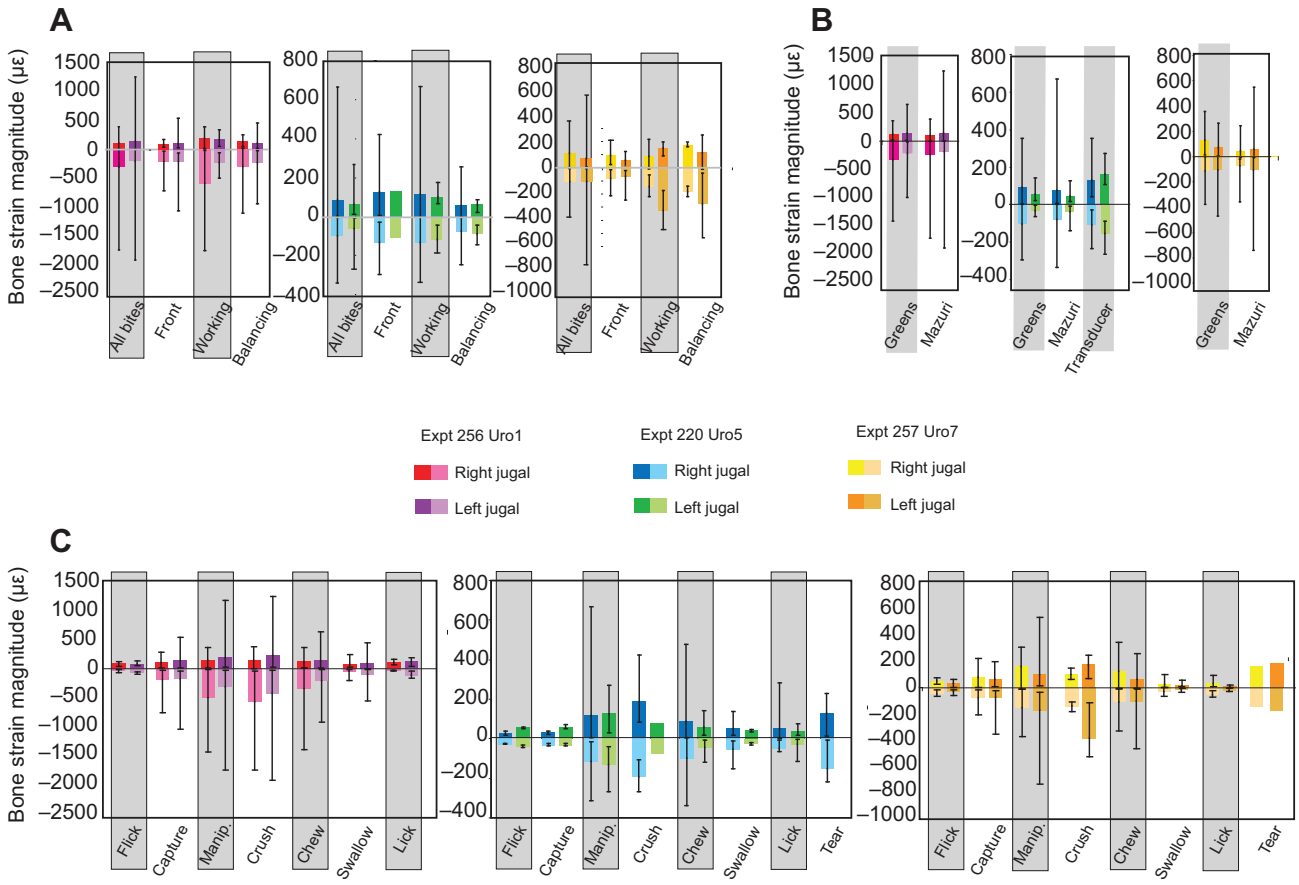

Fig. 1. Principal (ε_1 and ε_2) bone strain magnitudes (με) collected at right and left jugal sites in three *in vivo* experiments. Data are sorted by bite point (A), food type (B) and feeding behavior (C); data for all recorded cycles are also shown (A). Bars indicate mean principal strain magnitudes; whiskers indicate peak strain magnitudes. Note that scales vary between experiments.

foods (supplementary material Table S8) and between different feeding behaviors (supplementary material Table S9).

Two-way ANOVA confirms the significant effect of feeding behavior on ε_1 orientation at both gage sites in Uro1 and Uro7 (supplementary material Table S12); additionally, it suggests that food type impacted strain orientations in Uro1 and the right jugal of Uro7. There were significant effects of bite location on ε_1 orientation in Uro5 and Uro7 but not in Uro1 (supplementary material Table S13).

Shear strain

Within-gage means of shear strain range from 124 to 1013 με, with the grand mean for all gage sites in all three individuals being 382 με. Peak shear strains recorded for each animal were 3195 με (Uro1), 981 με (Uro5) and 1661 με (Uro7). Two-way ANOVA (supplementary material Table S10) revealed significant effects of food type and feeding behavior on shear strain magnitude at right gage sites; at left gage sites, feeding behavior and the interaction between food type and behavior significantly impacted shear strain magnitude. ANOVA testing for differences in shear strain magnitudes due to bite location revealed significant effects at both gage sites (supplementary material Table S11).

Bite force

The highest bite force produced by Uro5 was 31.4 N; mean bite force over 39 transducer bites was 12.5 N. These values are substantially lower than those reported in the similarly sized *U. acanthinurus* (59 N) or predicted in MDA models of *U. hardwickii* (51 N) (Herrel and DeVree, 2009; Moazen et al., 2008b). Most transducer bites occurred at the front of the jaws, although a small number of posterior bites were recorded; mean bite force recorded during posterior bites was higher (18.0 N) than during anterior bites (12.2 N). Bites were not prolonged; in some trials, several bites were delivered in quick succession. When bite force is plotted against simultaneously recorded maximum and minimum principal strains (Fig. 3), there is a positive correlation between bite force and both ε_1 and ε_2 strain magnitudes for left and right gage sites.

DISCUSSION

We have presented new *in vivo* bone strain data from the cranium of *U. geyri*, the first herbivorous sauropsid and third species of lizard from which such data have been collected. Additionally, bone strain and bite force were recorded simultaneously for one *U. geyri* individual. These data were collected in order to: document *in vivo* bone strains during feeding in *U. geyri*; understand the impact of food type, bite location, feeding behavior and individual variation on bone strains; compare cranial strain magnitudes in *U. geyri* during feeding with those documented in other taxa; and document bite forces in *U. geyri*.

Some problems with the data set should be noted. First, only three *U. geyri* were of sufficient size for the collection of bone strain data (and only one of these was willing to bite on a force transducer), resulting in a small sample size. Second, owing to animal behavior and occasional gage failure, complete data sets are not available for

The Journal of Experimental Biology (2014) doi:10.1242/jeb.096362

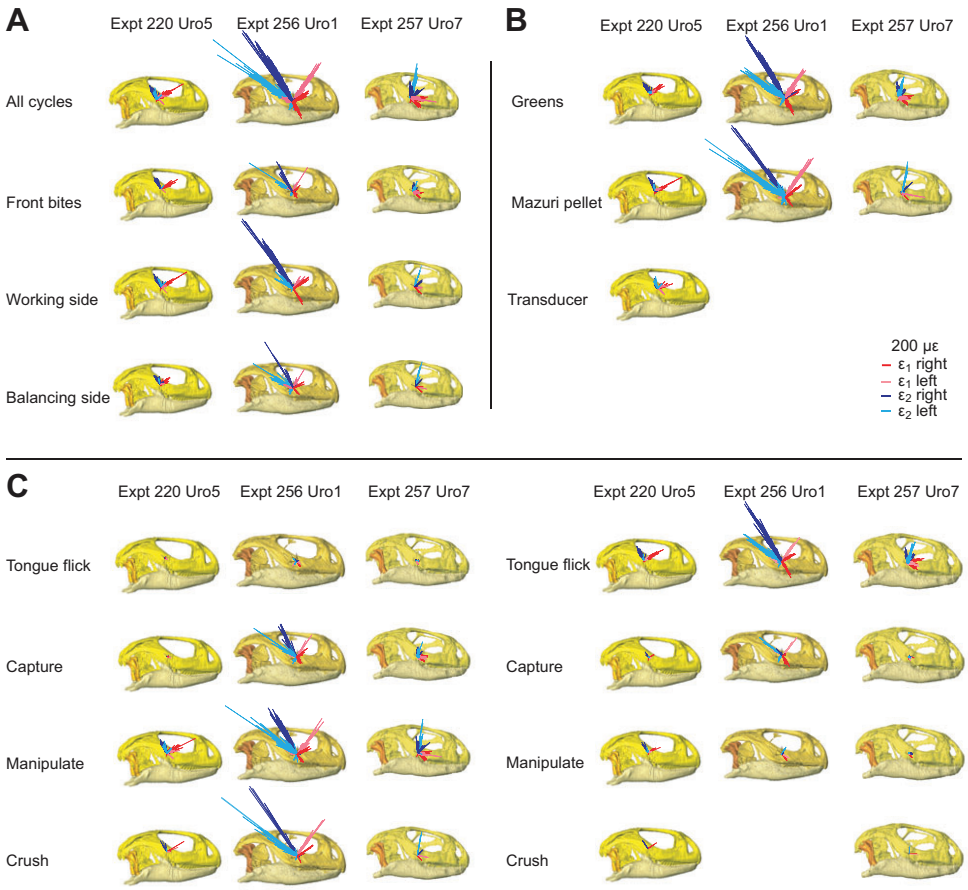

Fig. 2. Orientations of maximum (ε_1) and minimum (ε_2) principal strains at right and left gage sites (see inset) in three *Uromastyx geyri* individuals. Left side strains are shown from the right for ease of comparison. Vector lengths correspond to principal strain magnitude, see scale bars; all vectors are shown to the same scale. Strain vectors are sorted by bite location (A), food type (B) and feeding behavior (C). Top row in A shows strain orientations for all recorded cycles.

all experiments. Third, bone strains were collected from a single (bilateral) location – the jugal – as this was the only surface large enough to accommodate a gage that was also free of overlying muscle. Despite these drawbacks, our data set presents a substantial advance in our understanding of lizard cranial function during feeding.

Variations in principal strain orientations in *U. geyri*

Mean principal strain orientations were remarkably consistent within individual *U. geyri* when all cycles were considered. ε_1 orientation in the two males (Uro1 and Uro5) was anterodorsally directed in both the right and left jugal, suggesting compression of the postorbital bar along its long axis. In contrast, ε_1 was anteroventrally directed in the female *U. geyri* (Uro7), suggesting anteroposteriorly aligned tension in the ventral jugal and shear in the postorbital bar. This overall intra-individual consistency in principal strain orientations cannot be attributed to local muscle forces as no muscles attach in this area; instead, it may reflect the overall deformation regime of the skull. Inter-individual variation is attributable to variation in gage location, skeletal morphology, bone material properties and feeding behavior.

Nonetheless, closer examination revealed two distinct strain regimes at nearly every gage site. Data were sorted to reveal the factors responsible for the underlying signal. In four of six gage sites, frontal bites generated ε_1 strains rotated clockwise compared with posterior bites. This suggests that the postorbital bar is compressed parallel to its long axis during posterior bites, but not anterior bites. In their FEA of the *U. hardwickii* skull, Moazen et al. (Moazen et al., 2008a) found increased strain in the jugal (along with decreased strain in the skull roof) during posterior bites compared with anterior bites. They suggested that anterior bites induce compression in the bones of the snout and skull roof; in contrast, stress passes through the lateral aspect of the skull, including the jugal, during posterior bites. Our results are consistent with FEM predictions.

The clearest separation of the strain regimes occurred when data were sorted by behavior. ε_1 strains were rotated clockwise during tongue flicks and capture cycles (four of six sites) and lick and swallow cycles (five of six sites) compared with manipulation, crushing and chewing cycles.

For Uro1 and Uro7, ε_1 orientation was less variable during posterior bites than frontal bites, possibly because of the anterior jaws being used in more unpredictable behaviors. Circular–linear analyses reveal correlations between strain orientation and magnitude in Uro1 and Uro7 (supplementary material Tables S4–S6); such correlations are expected as there can only be one loading/strain regime during maximal contraction of the jaw muscles.

The difference in mean ε_1 orientation between male and female *U. geyri* was consistent for both sides of the head. Comparison of gage locations using CT scans and radiographs rules out the possibility that this was due to subtle differences in gage position. It is possible that variations in bone material properties may be responsible; this suggestion awaits testing. When compared with the smaller male (Uro5), the female (Uro7) exhibits a relatively shorter head, more rounded skull table and more vertical postorbital bar (Fig. 4); these differences are more pronounced when Uro7 is compared with the large male (Uro1). Differences in bite force and diet have been attributed to sexual dimorphism in lizard skulls (Herrel et al., 2001a; Herrel et al., 2001b; Kaliontzopoulou et al.,

The Journal of Experimental Biology (2014) doi:10.1242/jeb.096362

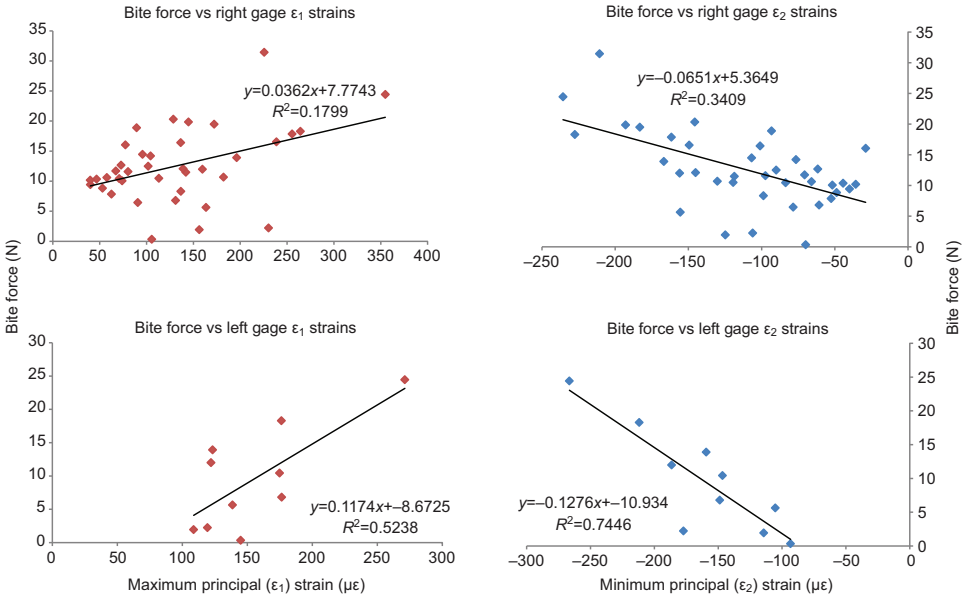

Fig. 3. Bite force plotted against simultaneously recorded maximum (left column) and minimum (right column) principal strain magnitudes for 39 transducer bites in Uro5 (Experiment 220). Top row is strain data measured at the right gage; bottom row is data measured at the left gage. (Note that because of gage failure, a larger number of data points are available for the right gage than the left gage.)

2012; Lappin et al., 2006), and it is not surprising that dimorphism would lead to differences in loading and strain regimes in males and females of the same species, although this study is the first to document such a difference. Because of the small sample size (two males and one female), further experiments are needed to confirm these results.

Strain magnitudes in *U. geyri* and comparisons with other taxa

Strain magnitudes (Fig. 1) and results from ANOVAs suggest that inter-individual effects have the greatest impact on principal and shear strain magnitudes in the *U. geyri* cranium during feeding, followed by feeding behavior, bite location and food type.

Mean strain magnitudes across all three *U. geyri* were 102 με (ε_1), −147 με (ε_2) and 382 με (shear), with peak principal strains exceeding ±500 με in Uro5 and Uro7 and approaching −2000 με in Uro1. Peak shear strains approached or exceeded 1000 με in Uro5 and Uro7 and exceeded 3000 με in Uro1. Mean principal strains in the *Alligator* skull frequently approached 1000 με (Metzger et al., 2005; Porro et al., 2013). Thus, mean principal in the cranium of *U. geyri* are not as high as those reported in *A. mississippiensis*; however, the latter is a carnivorous taxon that captures and subdues live, active prey (often with violent shaking or rolling). In contrast, *Uromastyx* is an herbivore not accustomed to biting defensively (although male *Uromastyx* do fight vigorously). It is possible that during the course of our experiments we did not elicit behaviors that resulted in near-maximum cranial bone strains. Alternatively, it is possible that *Uromastyx* crania are normally subjected to lower bone strain magnitudes during feeding. The higher safety factor may serve to protect the cranium against fatigue failure associated with the repetitive loading associated with herbivory. The importance of repetitive loading is also reflected in the fact that *Uromastyx* jaw elevator muscles contain more slow fibers than insectivorous lizard species (Herrel et al., 1998).

Comparisons with mammals are complicated by differences in skull shape and muscle attachments. Mean principal strains recorded from the maxilla of sheep during feeding were typically less than ±100 με, with peak strains around ±300 με (Thomason et al., 2001).

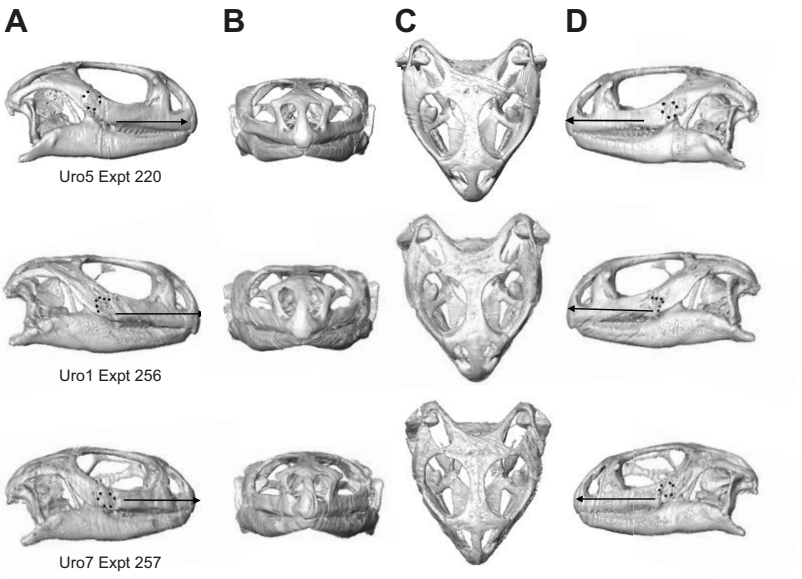

Fig. 4. 3D renderings of the skulls of the three *Uromastyx geyri* individuals used to collect *in vivo* bone strain data. Images were generated from CT scans (Gamma Medica Flex Triumph Imaging System, Department of Radiology, University of Chicago Medical Center) in Amira 5.4.2 (Visage Imaging, Berlin, Germany). Skulls are shown in right lateral (A), frontal (B), dorsal (C) and left lateral (D) views. Uro5 (top) and Uro1 (center) are male; Uro7 (bottom) is female. Lateral views illustrate the position and orientation of bone strain gages (black dots) and the reference axis (black arrow aligned with the anterior palate) that was used to standardize principal strain orientations across gage sites and experiments.

Mean principal strains recorded from the maxilla of pigs during mastication ranged from ±100 to ±300 με, while strains from the zygomatic arch were higher (Herring et al., 2001). Principal strains from the zygomatic arch of the hyrax during feeding rarely exceeded ±300 με (Lieberman et al., 2004), but in individual primates they average greater than 900 με, and can reach over 2000 με (Hylander and Johnson, 1997). However, it should be noted that the zygomatic arch of mammals is the site of origin for the masseter, unlike the jugal of reptiles. Thus, it would appear that the cranium of *U. geyri* experiences strain magnitudes similar to, if not higher than, those of sampled herbivorous mammals.

Strain variability due to food type

Feeding on greens produced higher mean principal strains whereas feeding on Mazuri pellets resulted in higher peak strains (Fig. 1). Furthermore, at five of six gage sites, mean ε_1 orientations are rotated counterclockwise during feeding on greens compared with feeding on Mazuri pellets (supplementary material Tables S1–S3). Differences in feeding behavior can explain these patterns. Although the average total number of cycles in a feeding sequence did not differ with changes in food, animals used a larger number of manipulation cycles when eating greens. In contrast, ingestion of Mazuri pellets involved more licking cycles and only pellets elicited crushing. At four of six gage sites, crushing produced higher strains than manipulation; as a result, pellet feeding sequences exhibited higher peak strains. However, no more than two crushing cycles were used during a feeding sequence, and the large number of low-magnitude licking cycles resulted in lower mean strains. Feeding sequences on greens involved more high-magnitude manipulation cycles, resulting in higher mean strains. Manipulation cycles exhibited ε_1 orientations rotated counterclockwise relative to licking cycles at five of six gage sites; again, the different number of manipulation and licking cycles employed while processing different foods explains the mean overall strain orientations of these feeding sequences.

Why do *Uromastyx* change their feeding behavior with different foods? Manipulation cycles are more frequent during feeding on greens because of the larger size of the food item – as a portion of the leaf is reduced, manipulation cycles are used to bring a ‘fresh’ portion to the posterior tooth row. Fracture of the pellet (into many small fragments) during crushing results in more licking cycles. Crushing is employed to break down pellets (but not leaves) because of differences in their material properties: pellets are substantially harder and more brittle than leaves. Thus, differences in food size and material properties elicit changes in feeding behavior, which in turn result in different strain regimes in the jugal. These findings bolster the suggestion by Ross et al. (Ross et al., 2012) that a better understanding of the relationship between variables (including food properties, behavior and strain patterns) is necessary to elucidate the link between diet and skull morphology.

Concluding remarks

The results presented here document *in vivo* bone strain in an herbivorous sauropsid for the first time. In addition to bone strain and bite force, 3D kinematic data, videofluoroscopic recordings and electromyographic data of jaw elevator muscles were obtained during these experiments and from an additional three *U. geyri* individuals. These results will be presented elsewhere and will be used to develop, refine and validate FEMs and MDA models of this taxon. Furthermore, the experiments described here are part of a larger collaborative study to collect *in vivo* experimental data from a range of lizard taxa exhibiting diverse skull and dental morphology, diets and feeding strategies (Gröning et al., 2013). The ultimate aim of these experiments and modeling efforts will be to quantitatively link specific variations in skull anatomy to varying functional demands in lepidosaurs.

The data presented here suggest that feeding behavior had greater impact on cranial strain orientation and magnitude than food type, highlighting the importance of sampling a wide range of behaviors to appreciate the stress, strain and loading regimes experienced by vertebrate skulls.

MATERIALS AND METHODS

Animal husbandry

Bone strain data were collected from three adult Saharan *Uromastyx geyri* housed at the University of Chicago (IL, USA). Subjects included two males, Uro1 [231 g; head length (HL, measured from premaxilla to posterior tip of squamosal) 36 mm] and Uro5 (212 g; HL 35 mm), and one female, Uro7 (202 g; HL 34 mm). Animals were housed individually or in sexed pairs in large (152×60×60 cm) molded plastic cages (Showcase Cages, Lake Elsinore, CA, USA) in a temperature-controlled room set at 21–24°C on a 12 h:12 h light:dark cycle. A basking spot at higher temperature (up to 49°C) was available to the animals. Once daily, animals were provided with leafy greens (lettuce, endive, bok choy, mustard greens) and Mazuri brand tortoise pellets *ad libitum*. Animals were kept on a substrate of white millet seed that was occasionally ingested intentionally with no ill effects. All husbandry and experimental procedures were in accordance with federal regulations and approved Institutional Animal Care and Use Committee protocols.

Data collection

Bone strain data were recorded during three separate experiments (Table 1) using either stacked rectangular rosette strain gages (Uro1) (FRA 1-11-1L; Texas Measurements, Inc., College Station, TX, USA) or stacked delta rosette strain gages (Uro5 and Uro7) (SA-06-030WY-120; Vishay Precision Group Micro-Measurements, Raleigh, NC, USA). The gages were wired, insulated and sterilized with hydrogen peroxide gas using methods previously described (Ross, 2001; Ross et al., 2011). The lateral surface of the postorbital bar (formed by the jugal), which is located ventral and posterior to the orbit (Fig. 4), provided the only bone surface large enough for gage placement that was free of overlying jaw muscles. For all three animals, gages were placed on the lower portion of the jugal on both sides of the head. Gage positions and orientations were recorded using photographs, CT scans and radiographs (Fig. 4).

Animals were food-deprived for 24 h prior to surgery and anesthetized using an intramuscular injection of ketamine (15 mg kg^{-1} body mass) and dexmedetomidine (100 μg kg^{-1} body mass). After anesthesia, <1 cm^2 of skin overlying the jugal gage sites was removed, the periosteum elevated to expose the bone, the bone degreased with 100% chloroform, and the gage bonded to the surface of the bone using cyanoacrylate adhesive. To prevent movements of the lead wires causing strain in the gage, wires were glued to the skin for ~1 cm using the same adhesive, gathered together and shallowly sutured to loose skin on the back. Anesthesia was reversed with atipamezole (100 μg kg^{-1} body mass) and the animals were returned to temporary

Table 1. Experimental summary, including recording method, subject and gage information, and number of cycles analyzed

Experiment no., type	Individual ID, gender	Gage type	Gage locations	Recording frequency (Hz)	Total cycles
220, Vicon	Uro5, male	Delta rosettes	Bilateral, jugal bone	2000	395
256, Videofluoroscopy	Uro1, male	Rectangular rosettes	Bilateral, jugal bone	5000	629
257, Videofluoroscopy	Uro7, female	Delta rosettes	Bilateral, jugal bone	5000	339

housing tanks to recover and for the duration of data collection. Data were collected twice daily (for up to 5 days) in sessions lasting no more than 2 h or until the animals stopped feeding.

The animals were fed in a clear Plexiglas tunnel (60×10×10 cm) while strain data were collected. For Uro5, experiments were recorded using a digital video camera; for Uro1 and Uro7, experiments were recorded using videofluoroscopy (General Electric OEC 9600 Series C-Arm, Fairfield, CT, USA). In both cases, strain data could be attributed to food type, bite location and feeding behavior. Voltage changes in the strain gages were conditioned and amplified on Vishay Micro-Measurements 2310A signal conditioning bridge-amplifiers while the animals fed on assorted greens (lettuce, endive and mustard greens) and Mazuri pellets. Food items were placed on the floor of the tunnel in front of the animals using tongs; occasionally, animals began eating while the item was held in the tongs. For Uro5, data were acquired at 2000 Hz and acquisition to PC was controlled by Vicon Nexus 1.6 Software (Vicon, Los Angeles, CA, USA). For Uro1 and Uro7, data were acquired at 5000 Hz through a National Instruments DAQ board run by MiDAS 2.0 Digital Video and Data Capture Software (Xcitex, Inc., Cambridge, MA, USA) and were saved to a PC for subsequent analysis.

Uromastyx geyri are not aggressive biters and bite force was obtained from only one individual (Uro5). *In vivo* bite forces were measured using a Kistler force transducer (Type 9203, range ±500 N; Kistler, Switzerland) connected to a Kistler charge amplifier (Type 5995) connected to an A-D system producing an output in voltage. Uro5 was manually restrained at the pectoral and pelvic girdles. The head was unrestrained during transducer bites; thus, deformation of the skull is attributed to muscle and bite reaction forces only.

Bone strain data extraction

Strain gage outputs were filtered and processed in IGOR Pro 4.0.4 (WaveMetrics, Inc., Lake Oswego, OR, USA) using custom-written software and calibration files produced during the recording sessions. The strain data (strain being a dimensionless unit, ε, that represents change in length over original length, $\Delta L/L$) were converted to με. The strain tracings (along with simultaneous video/videofluoroscopy and electromyograms) were examined to identify movement artifacts; these sequences were not included in the analysis. The magnitude of the maximum (ε_1) and minimum (ε_2) principal strains were calculated for every cycle recorded (Hibbeler, 2000); mean and peak principal strains recorded at each gage site in each experiment are recorded in Fig. 1 and supplementary material Tables S1–S3, sorted by bite location, food type and behavior. ε_1 is the largest tensile (or occasionally least negative) strain and usually registers as a positive value; ε_2 is the largest compressive (or occasionally least tensile) strain and usually registers as a negative value. The orientation of ε_1 relative to the A-element of the strain gage was calculated for each cycle (the orientation of ε_2 is orthogonal to that of ε_1), as was the ratio of maximum to minimum principal strains $|\varepsilon_1/\varepsilon_2|$; values are presented in supplementary material Tables S1–S3. Shear strain (γ), which is equal to $\varepsilon_1-\varepsilon_2$, was also calculated for each cycle.

To facilitate comparisons between gage sites and experiments, strain orientations presented in all tables and figures (and used in statistical analyses) were calculated with the skull in right lateral view (thus, left side strains are seen from 'below'). Strain orientations were calculated relative to the axes shown in Fig. 4; the reference axis (horizontal) is aligned with the palate in lateral view and is directed anteriorly whereas the vertical axis is perpendicular to this and points dorsally. By convention, positive values are rotated counterclockwise from the reference axis (vectors rotated clockwise from the axis are negative). Custom software within IGOR Pro 4.0 was used to convert strain orientations and magnitudes to vectors within polar coordinates. Vector plots (Fig. 2), in which the orientations and relative magnitudes of ε_1 and ε_2 during all recorded bites (as well as sorted by bite location, food type and behavior) are displayed, were created using Adobe Illustrator CS 5.1 (Adobe Systems Incorporated, San Jose, CA, USA).

Bite force extraction

The force transducer used in Experiment 220 (Uro5) was calibrated by hanging weights of known mass from the transducer and recording the output voltage. The resulting linear regression ($y=38.015x+0.2635$; $R=0.9964$) was used to convert voltage to bite force. Bite force was plotted against simultaneously recorded maximum principal strains (ε_1 and ε_2) from both right and left gage sites (Fig. 3).

Statistical analyses of bone strain data

To quantify the effects of various factors on strain magnitude and orientation, data from left and right gage sites were sorted by bite location (front, working side or balancing side), food type (greens, Mazuri pellets or force transducer) and feeding behavior. Missing data indicate that no strains were recorded for a particular bite location, food type or behavior.

Principal strain orientations are axial circular data in which an ε_1 orientation of 0 deg is equal to 180 deg (and thus 90 deg is not a sensible mean). These data cannot be analyzed using traditional statistics. Quantitative analyses of *in vivo* principal strain orientations were performed in Oriana 3.13 (Kovach Computing Services, Anglesey, UK). In order to conduct these analyses, all angle data had to be converted to positive values (e.g. −30 deg was converted to 330 deg prior to analysis). Additionally, Oriana converts all axial data to values between 0 and 180 deg. Readers are urged to note these changes when comparing descriptive statistics from supplementary material Tables S1–S3 with circular statistics from supplementary material Tables S4–S6.

Descriptive circular statistics (supplementary material Tables S4–S6) were produced for ε_1 orientations at each gage site, with data grouped by bite location, food type and behavior. Groups containing a single data point (see supplementary material Tables S1–S3) were excluded from statistical analyses. The statistics presented here include: the mean angle of the vectors (μ) relative to the reference axis describe above; the length of the mean vector (r) ranging from 0 to 1, which is a measure of angular dispersion with values closer to 1 indicating that individual observations are clustered more closely around the mean (length of mean vector is not the mean magnitude of ε_1); the concentration (k), which measures the departure of the distribution from a uniform distribution (or perfect circle) and was calculated using published formulas (Fisher, 1993; Mardia and Jupp, 2000); the circular variance (V), which is calculated as $V=1-r$, and is equivalent to its linear counterpart; the circular standard deviation (S), calculated as $S=[-2\times\ln(r)]^{1/2}$; the standard error of the mean; and the 95% and 99% confidence intervals derived from standard error. Additionally, Rayleigh's test of uniformity and Watson's U^2-test were used to determine whether data are derived from a von Mises distribution (continuous probability distribution on a circle, not to be confused with von Mises stress). To determine whether ε_1 strain orientations changed as strain magnitude increased, circular–linear correlation coefficients were calculated between ε_1 orientation and magnitude (Zar, 1999) (supplementary material Tables S4–S6). To determine whether the distribution of ε_1 angles differ significantly with changes in bite location, food type or feeding behavior, ε_1 orientations recorded within each gage were compared using a non-parametric Mardia–Watson–Wheeler test or a parametric Watson–Williams F-test (supplementary material Tables S7–S9). (These tests determine whether two or more distributions are identical; significant differences between distributions will lead to a large W test statistic and low probability of distributions being identical.)

Mixed-model ANOVAs were used to investigate the effect of bite location, food type and feeding behavior on principal and shear strain magnitudes, and principal strain orientations in JMP 8 (SAS Institute, Cary, NC, USA) using the restricted maximum likelihood method, with individuals as random effects and food, behavior and their interaction as fixed effects (supplementary material Table S10). Because strain magnitude distribution was skewed, data were log-transformed to normalize them. Separate analyses were run for right and left gages; gage sites and behaviors with few data points were excluded. Because bite location was identified in only a third of all cycles, separate mixed-model ANOVAs were conducted for bite location with individuals as random effects (supplementary material Table S11). Tukey *post hoc* comparisons of differences in means were carried out. Significance was assessed at $\alpha=0.05$. Angular data were analyzed using the CircStat (Berens, 2009) toolbox in MATLAB (MathWorks, Natick, MA, USA). Analyses were performed in the same groupings as above; however, because we cannot include individual

variation as a random effect, we tested each individual independently. The effect of food type and behavior was analyzed using the Harrison–Kanji test (supplementary material Table S12). Depending on the concentration parameter, κ, two different statistics were used [χ^2 and F for large κ; when κ is small, the interaction effect is not reported; see Harrison and Kanji (Harrison and Kanji, 1988)]. To test the effect biting side on strain orientation, we used the Watson–Williams test (supplementary material Table S13).

Acknowledgements
Michael Alcorn, Kate Fagan, Kathryn Murray, and Sawyer Kisken provided technical support and assisted during experiments. Maggie Bruner, Jennifer McGrath, Marek Niekrasz, Karin Peterson and Elizabeth Theriault assisted with animal husbandry and provided veterinary care. *Uromastyx* were CT-scanned by Chad Haney.

Competing interests
The authors declare no competing financial interests.

Author contributions
L.B.P., C.F.R., S.E.E. and M.J.F. conceived of and designed the research. L.B.P. and J.C.O.R. cared for research animals. L.B.P., C.F.R., J.I.D. and J.C.O.R. collected *in vivo* data. L.B.P., C.F.R. and J.I.D. processed and interpreted *in vivo* data. L.B.P. and C.F.R. drafted the manuscript. All authors read and commented on the manuscript.

Funding
Funding was provided by joint Biotechnology and Biological Sciences Research Council grants [BB/H011668/1, BB/H011854/1] to M.J.F. and S.E.E. Salary support for L.B.P. was provided by the Pritzker School of Medicine, University of Chicago. Deposited in PMC for immediate release.

Supplementary material
Supplementary material available online at
http://jeb.biologists.org/lookup/suppl/doi:10.1242/jeb.096362/-/DC1

References

Berens, P. (2009). CircStat: a Matlab toolbox for circular statistics. *J. Stat. Softw.* **31**, available at: http://www.jstatsoft.org/v31/i10.
Crompton, A. W. (1989). The evolution of mammalian mastication. In *Complex Organismal Functions: Integration and Evolution in Vertebrates* (ed. D. B. Wake and G. Roth), pp. 23-40. New York, NY: John Wiley and Sons Ltd.
Curtis, N., Jones, M. E. H., Shi, J., O'Higgins, P., Evans, S. E. and Fagan, M. J. (2011). Functional relationship between skull form and feeding mechanics in *Sphenodon*, and implications for diapsid skull development. *PLoS ONE* **6**, e29804.
Curtis, N., Jones, M. E. H., Evans, S. E., O'Higgins, P. and Fagan, M. J. (2013). Cranial sutures work collectively to distribute strain throughout the reptile skull. *J. R. Soc. Interface* **10**, 20130442.
Fisher, N. I. (1993). *Statistical Analysis of Circular Data*. Cambridge: Cambridge University Press.
Gröning, F., Jones, M. E. H., Curtis, N., Herrel, A., O'Higgins, P., Evans, S. E. and Fagan, M. J. (2013). The importance of accurate muscle modelling for biomechanical analyses: a case study with a lizard skull. *J. R. Soc. Interface* **10**, 20130216.
Harrison, D. and Kanji, G. K. (1988). The development of analysis of variance for circular data. *J. Appl. Statist.* **15,** 197-223.
Heesy, C. P. (2005). Function of the mammalian postorbital bar. *J. Morphol.* **264**, 363-380.
Herrel, A. and De Vree, F. (1999). Kinematics of intraoral transport and swallowing in the herbivorous lizard uromastix acanthinurus. *J. Exp. Biol.* **202**, 1127-1137.
Herrel, A. and De Vree, F. (2009). Jaw and hyolingual muscle activity patterns and bite forces in the herbivorous lizard *Uromastyx acanthinurus*. *Arch. Oral Biol.* **54**, 772-782.
Herrel, A., Cleuren, J. and Vree, F. (1997). Quantitative analysis of jaw and hyolingual muscle activity during feeding in the lizard *Agama stellio*. *J. Exp. Biol.* **200**, 101-115.
Herrel, A., Timmermans, J.-P. and De Vree, F. (1998). Tongue flicking in agamid lizards: morphology, kinematics, and muscle activity patterns. *Anat. Rec.* **252**, 102-116.
Herrel, A., De Grauw, E. and Lemos-Espinal, J. A. (2001a). Head shape and bite performance in xenosaurid lizards. *J. Exp. Zool.* **290**, 101-107.
Herrel, A., Van Damme, R., Vanhooydonck, B. and De Vree, F. (2001b). The implications of bite performance of diet in two species of lacertid lizards. *Can. J. Zool.* **79**, 662-670.
Herrel, A., Vanhooydonck, B. and Van Damme, R. (2004). Omnivory in lacertid lizards: adaptive evolution or constraint? *J. Evol. Biol.* **17**, 974-984.
Herrel, A., Schaerlaeken, V., Meyers, J. J., Metzger, K. A. and Ross, C. F. (2007). The evolution of cranial design and performance in squamates: consequences of skull-bone reduction on feeding behavior. *Integr. Comp. Biol.* **47**, 107-117.
Herring, S. W. and Teng, S. (2000). Strain in the braincase and its sutures during function. *Am. J. Phys. Anthropol.* **112**, 575-593.
Herring, S. W., Rafferty, K. L., Liu, Z. J. and Marshall, C. D. (2001). Jaw muscles and the skull in mammals: the biomechanics of mastication. *Comp. Biochem. Physiol.* **131A**, 207-219.
Hibbeler, R. C. (2000). *Mechanics of Materials*. Upper Saddle River, NJ: Prentice Hall.
Hylander, W. L. and Johnson, K. R. (1992). Strain gradients in the craniofacial region of primates. In *The Biological Mechanisms of Tooth Movement and Craniofacial Adaptation* (ed. Z. Davidovich), pp. 559-569. Columbus, OH: The Ohio State University.
Hylander, W. L. and Johnson, K. R. (1997). In vivo bone strain patterns in the zygomatic arch of macaques and the significance of these patterns for functional interpretations of craniofacial form. *Am. J. Phys. Anthropol.* **102**, 203-232.
Hylander, W. L., Johnson, K. R. and Crompton, A. W. (1987). Loading patterns and jaw movements during mastication in *Macaca fascicularis*: a bone-strain, electromyographic, and cineradiographic analysis. *Am. J. Phys. Anthropol.* **72**, 287-314.
Hylander, W. L., Picq, P. G. and Johnson, K. R. (1991a). Masticatory-stress hypotheses and the supraorbital region of primates. *Am. J. Phys. Anthropol.* **86**, 1-36.
Hylander, W. L., Picq, P. G. and Johnson, K. R. (1991b). Function of the supraorbital region of primates. *Arch. Oral Biol.* **36**, 273-281.
Kaliontzopoulou, A., Adams, D. C., van der Meijden, A., Perera, A. and Carretero, M. A. (2012). Relationships between head morphology, bite performance and ecology in two species of *Podarcis* wall lizards. *Evol. Ecol.* **26**, 825-845.
Lappin, A. K., Hamilton, P. S. and Sullivan, B. K. (2006). Bite-force performance and head shape in a sexually dimorphic crevice-dwelling lizard, the common chuckwalla (*Sauromalus ater* (= *obesus*)). *Biol. J. Linn. Soc. Lond.* **88**, 215-222.
Lieberman, D. E., Krovitz, G. E., Yates, F. W., Devlin, M. and St Claire, M. (2004). Effects of food processing on masticatory strain and craniofacial growth in a retrognathic face. *J. Hum. Evol.* **46**, 655-677.
Mardia, K. V. and Jupp, P. (2000). *Directional Statistics*. New York, NY: John Wiley and Sons Ltd.
Metzger, K. A. (2002). Cranial kinesis in lepidosaurs: skulls in motion. In *Topics in Functional and Ecological Vertebrate Morphology* (ed. P. Aerts, K. D'Août, A. Herrel and R. Van Damme), pp. 15-46. Maastricht: Shaker Publishing.
Metzger, K. A. and Herrel, A. (2005). Correlations between lizard cranial shape and diet: a quantitative, phylogenetically informed analysis. *Biol. J. Linn. Soc. Lond.* **86**, 433-466.
Metzger, K. A., Daniel, W. J. T. and Ross, C. F. (2005). Comparison of beam theory and finite-element analysis with *in vivo* bone strain data from the alligator cranium. *Anat. Rec.* **283A**, 331-348.
Moazen, M., Curtis, N., Evans, S. E., O'Higgins, P. and Fagan, M. J. (2008a). Combined finite element and multibody dynamics analysis of biting in a *Uromastyx hardwickii* lizard skull. *J. Anat.* **213**, 499-508.
Moazen, M., Curtis, N., Evans, S. E., O'Higgins, P. and Fagan, M. J. (2008b). Rigid-body analysis of a lizard skull: modelling the skull of *Uromastyx hardwickii*. *J. Biomech.* **41**, 1274-1280.
Moazen, M., Curtis, N., O'Higgins, P., Jones, M. E. H., Evans, S. E. and Fagan, M. J. (2009a). Assessment of the role of sutures in a lizard skull: a computer modelling study. *Proc. Biol. Sci.* **276**, 39-46.
Moazen, M., Curtis, N., O'Higgins, P., Evans, S. E. and Fagan, M. J. (2009b). Biomechanical assessment of evolutionary changes in the lepidosaurian skull. *Proc. Natl. Acad. Sci. USA* **106**, 8273-8277.
Porro, L. B., Metzger, K. A., Iriarte-Diaz, J. and Ross, C. F. (2013). *In vivo* bone strain and finite element modeling of the mandible of *Alligator mississippiensis*. *J. Anat.* **223**, 195-227.
Ravosa, M. J., Noble, V. E., Hylander, W. L., Johnson, K. R. and Kowalski, E. M. (2000a). Masticatory stress, orbital orientation and the evolution of the primate postorbital bar. *J. Hum. Evol.* **38**, 667-693.
Ravosa, M. J., Johnson, K. R. and Hylander, W. L. (2000b). Strain in the galago facial skull. *J. Morphol.* **245**, 51-66.
Rieppel, O. and Labhardt, L. (1979). Mandibular mechanics in *Varanus niloticus* (Reptilia: Lacertilia). *Herpetologica* **35**, 158-163.
Robinson, P. L. (1976). How *Sphenodon* and *Uromastyx* grow their teeth and use them. In *Morphology and Biology of Reptiles* (ed. A. d'A. Bellairs and C. B. Cox), pp. 43-64. Waltham, MA: Academic Press.
Ross, C. F. (1995a). Allometric and functional influences on primate orbit orientation and the origins of the Anthropoidea. *J. Hum. Evol.* **29**, 201-227.
Ross, C. (1995b). Muscular and osseous anatomy of the primate anterior temporal fossa and the functions of the postorbital septum. *Am. J. Phys. Anthropol.* **98**, 275-306.
Ross, C. F. (2001). *In vivo* function of the craniofacial haft: the interorbital 'pillar'. *Am. J. Phys. Anthropol.* **116**, 108-139.
Ross, C. F. and Hylander, W. L. (1996). *In vivo* and *in vitro* bone strain in the owl monkey circumorbital region and the function of the postorbital septum. *Am. J. Phys. Anthropol.* **101**, 183-215.
Ross, C. F. and Metzger, K. A. (2004). Bone strain gradients and optimization in vertebrate skulls. *Ann. Anat.* **186**, 387-396.
Ross, C. F., Patel, B. A., Slice, D. E., Strait, D. S., Dechow, P. C., Richmond, B. G. and Spencer, M. A. (2005). Modeling masticatory muscle force in finite element analysis: sensitivity analysis using principal coordinates analysis. *Anat. Rec.* **283A**, 288-299.
Ross, C. F., Eckhardt, A., Herrel, A., Hylander, W. L., Metzger, K. A., Schaerlaeken, V., Washington, R. L. and Williams, S. H. (2007). Modulation of intra-oral processing in mammals and lepidosaurs. *Integr. Comp. Biol.* **47**, 118-136.

Ross, C. F., Berthaume, M. A., Dechow, P. C., Iriarte-Diaz, J., Porro, L. B., Richmond, B. G., Spencer, M. and Strait, D. (2011). *In vivo* bone strain and finite-element modeling of the craniofacial haft in catarrhine primates. *J. Anat.* **218**, 112-141.

Ross, C. F., Iriarte-Diaz, J. and Nunn, C. L. (2012). Innovative approaches to the relationship between diet and mandibular morphology in primates. *Int. J. Primatol.* **33**, 632-660.

Schwenk, K. (2000). Feeding in lepidosaurs. In *Feeding: Form, Function and Evolution in Tetrapod Vertebrates* (ed. K. Schwenk), pp. 175-291. San Diego, CA: Academic Press.

Smith, K. K. and Hylander, W. L. (1985). Strain gauge measurement of mesokinetic movement in the lizard Varanus exanthematicus. *J. Exp. Biol.* **114**, 53-70.

Stayton, C. T. (2005). Morphological evolution of the lizard skull: a geometric morphometrics survey. *J. Morphol.* **263**, 47-59.

Stayton, C. T. (2006). Testing hypotheses of convergence with multivariate data: morphological and functional convergence among herbivorous lizards. *Evolution* **60**, 824-841.

Strait, D. S., Wang, Q., Dechow, P. C., Ross, C. F., Richmond, B. G., Spencer, M. A. and Patel, B. A. (2005). Modeling elastic properties in finite-element analysis: how much precision is needed to produce an accurate model? *Anat. Rec.* **283A**, 275-287.

Thomason, J. J., Grovum, L. E., Deswysen, A. G. and Bignell, W. W. (2001). *In vivo* surface strain and stereology of the frontal and maxillary bones of sheep: implications for the structural design of the mammalian skull. *Anat. Rec.* **264**, 325-338.

Throckmorton, G. S. (1974). *Oral Food Processing and Digestive Efficiency in Herbivorous Iguanid and Agamid Lizards*. PhD thesis, Committee on Evolutionary Biology, University of Chicago, IL, USA.

Throckmorton, G. S. (1976). Oral food processing in two herbivorous lizards, *Iguana iguana* (Iguanidae) and *Uromastix aegyptius* (Agamidae). *J. Morphol.* **148**, 363-390.

Throckmorton, G. S. (1978). Action of the pterygoideus muscle during feeding in the lizard *Uromastix aegyptius* (Agamidae). *Anat. Rec.* **190**, 217-222.

Throckmorton, G. S. (1979). The effect of wear on the cheek teeth and associated dental tissues of the lizard *Uromastix aegyptius* (Agamidae). *J. Morphol.* **160**, 195-207.

Throckmorton, G. S. (1980). The chewing cycle in the herbivorous lizard *Uromastix aegyptius* (Agamidae). *Arch. Oral Biol.* **25**, 225-233.

Verrue, V., Dermaut, L. and Verhegghe, B. (2001). Three-dimensional finite element modelling of a dog skull for the simulation of initial orthopaedic displacements. *Eur. J. Orthod.* **23**, 517-527.

Zar, J. H. (1999). *Biostatistical Analysis*. Upper Saddle River, NJ: Prentice Hall.

The Journal of Experimental Biology

Table S1. Descriptive statistics for principal (ε_1 and ε_2) strain magnitude, $|(\varepsilon_1/\varepsilon_2)|$, and ε_1 orientation for Experiment 220 (*Uro5*).

Gage location	Bite side/ Food/ Behavior	n	ε_1			ε_2			$\varepsilon_1/\varepsilon_2$ ratio		ε_1 orientation	
			Mean	S.D.	Max	Mean	S.D.	Max	Mean	S.D.	Mean	S.D.
Right jugal	All	395	91	85	668	-95	77	-337	2.84	26.31	25	29
	Front	53	132	86	424	-129	72	-293	1.04	0.37	25	12
	WS	123	122	94	668	-129	77	-337	1.21	1.94	28	22
	BS	102	62	58	256	-75	64	-245	7.09	51.58	15	41
	Greens	221	93	77	353	-105	79	-293	4.06	35.13	25	31
	Mazuri	129	77	97	668	-77	77	-337	1.30	1.92	28	28
	Transducer	39	132	71	355	-109	55	-236	1.22	0.41	23	12
	Flick	4	25	9	39	-26	2	-28	0.96	0.32	53	6
	Capture	4	29	8	37	-31	5	-37	0.94	0.18	53	3
	Manipulation	128	118	94	668	-116	76	-313	1.04	0.48	29	26
	Crush	5	188	151	424	-194	66	-269	0.89	0.45	22	10
	Chew	175	87	79	477	-98	75	-337	4.56	39.41	22	31
	Swallow	11	51	42	137	-53	49	-152	1.29	0.55	43	24
	Lick	46	49	57	284	-50	68	-265	2.60	5.28	24	31
	Tear	4	130	90	231	-152	98	-218	1.07	0.49	26	10
Left jugal	All	67	67	54	271	-57	57	-266	1.75	1.48	1	29
	Front	1	139	NA	139	-105	NA	-105	1.32	NA	-38	NA
	WS	8	109	36	177	-113	50	-186	1.08	0.38	9	24
	BS	5	66	25	90	-85	42	-137	0.82	0.18	15	6
	Greens	15	56	33	144	-36	19	-62	2.64	2.68	17	34
	Mazuri	41	46	27	127	-40	37	-137	1.59	0.77	-4	23
	Transducer	11	162	50	271	-154	55	-266	1.15	0.54	-2	35

Flick	4	56	4	61	-38	7	-44	1.50	0.36	-9	5
Capture	3	60	9	69	-30	6	-37	2.02	0.10	-14	1
Manipulation	17	124	56	271	-130	59	-266	0.98	0.25	9	27
Crush	1	74	NA	74	-75	NA	-75	0.98	NA	6	NA
Chew	10	60	45	144	-45	45	-120	1.90	0.68	6	31
Swallow	4	46	5	49	-20	7	-29	2.47	0.73	-10	5
Lick	19	33	15	75	-28	24	-114	2.00	2.37	-2	30

Table S2. Descriptive statistics for principal (ε_1 and ε_2) strain magnitude, $|(\varepsilon_1/\varepsilon_2)|$, and ε_1 orientation for Experiment 256 (*Uro1)*.

Gage location	Bite side/ Food/ Behavior	n	ε_1			ε_2			$\varepsilon_1/\varepsilon_2$ ratio		ε_1 orientation	
			Mean	S.D.	Max	Mean	S.D.	Max	Mean	S.D.	Mean	S.D.
Right jugal	All cycles	543	123	72	390	-311	360	-1751	1.97	3.38	0	43
	Front	25	102	31	188	-192	215	-706	1.59	1.54	-4	46
	WS	62	192	109	390	-588	446	-1751	1.02	1.72	18	37
	BS	25	136	59	251	-297	314	-1099	2.88	6.04	17	34
	Greens	415	127	73	373	-335	361	-1444	1.84	3.24	1	42
	Mazuri	128	108	69	390	-233	344	-1751	2.39	3.80	-4	46
	Flick	9	94	29	127	-29	19	-69	5.27	4.36	-41	27
	Capture	48	109	46	283	-184	222	-753	1.87	1.85	-10	43
	Manipulation	136	148	78	365	-505	368	-1444	0.88	1.49	18	32
	Crush	23	155	110	390	-574	548	-1751	0.49	0.65	27	27
	Chew	214	121	76	373	-332	347	-1397	1.47	2.70	10	41
	Swallow	91	91	41	252	-37	29	-198	4.63	5.64	-41	33
	Lick	9	112	29	166	-31	7	-40	4.01	1.95	-54	3
Left jugal	All cycles	629	149	151	1261	-208	219	-1934	1.08	1.17	26	44
	Front	28	116	93	550	-191	200	-1049	0.78	0.37	32	44
	WS	25	166	75	333	-239	116	-496	0.75	0.39	52	18
	BS	65	116	76	463	-220	180	-944	0.78	0.63	30	49
	Greens	421	154	110	667	-217	189	-1010	0.97	0.66	36	41
	Mazuri	208	141	163	1261	-188	269	-1934	1.30	1.79	7	43
	Flick	13	85	22	133	-69	14	-97	1.24	0.27	-2	40
	Capture	56	137	93	550	-178	196	-1049	1.08	0.57	14	44

Manipulation	143	199	153	1190	-307	249	-1755	0.85	0.69	47	33
Crush	36	236	267	1261	-418	401	-1934	0.68	0.72	53	26
Chew	230	139	107	637	-198	177	-923	1.03	0.96	36	42
Swallow	120	105	72	446	-94	93	-557	1.56	2.05	-8	36
Lick	18	123	34	192	-99	31	-163	1.27	0.23	-28	3

Table S3. Descriptive statistics for principal (ε_1 and ε_2) strain magnitude, $|(\varepsilon_1/\varepsilon_2)|$, and ε_1 orientation for Experiment 257 (*Uro7*).

Gage location	Bite side/ Food/ Behavior	n	ε_1			ε_2			$\varepsilon_1/\varepsilon_2$ ratio		ε_1 orientation	
			Mean	S.D.	Max	Mean	S.D.	Max	Mean	S.D.	Mean	S.D.
Right jugal	All	339	114	82	354	-104	77	-376	1.84	9.24	-29	34
	Front	30	95	52	211	-82	53	-213	1.39	0.58	-4	31
	WS	11	89	83	217	-144	63	-219	0.54	0.37	-46	13
	BS	5	176	13	189	-184	30	-220	0.97	0.14	-27	18
	Greens	275	130	78	354	-111	78	-376	2.14	10.24	-22	30
	Mazuri	64	44	54	242	-74	66	-358	0.57	0.30	-56	35
	Flick	10	51	17	80	-46	19	-66	1.26	0.54	-8	35
	Capture	51	86	62	226	-76	47	-209	1.19	0.61	-17	34
	Manipulation	103	165	74	314	-152	80	-376	1.24	0.78	-19	24
	Crush	4	105	37	154	-143	40	-183	0.77	0.28	-42	3
	Chew	108	130	80	354	-111	77	-333	1.72	3.20	-28	30
	Swallow	34	31	20	105	-30	16	-64	6.27	28.55	-59	39
	Lick	26	34	22	98	-53	16	-70	0.68	0.39	-55	37
	Tear	1	165	NA	165	-140	NA	140	1.18	NA	-42	NA
Left jugal	All	339	69	63	547	-105	113	-743	1.08	2.34	-26	35
	Front	30	59	29	125	-65	56	-245	1.14	0.61	-41	50
	WS	5	152	44	198	-324	112	-472	0.53	0.31	-13	6
	BS	11	113	83	252	-275	165	-534	0.37	0.15	-16	15
	Greens	275	72	50	265	-105	94	-472	1.04	1.83	-26	35
	Mazuri	64	56	101	547	-106	172	-743	1.21	3.84	-28	37

Flick	10	32	24	65	-28	15	-62	1.20	0.94	-33	56
Capture	51	63	42	200	-70	60	-359	1.07	0.58	-51	35
Manipulation	103	105	72	547	-170	122	-743	0.69	0.27	-15	20
Crush	4	175	79	252	-387	185	-534	0.48	0.10	-9	3
Chew	108	67	53	265	-105	103	-472	1.14	2.64	-24	33
Swallow	34	17	19	56	-15	11	-56	2.54	5.49	-37	51
Lick	26	9	5	20	-21	7	-30	0.50	0.34	-17	35
Tear	1	188	NA	188	-173	NA	-173	1.09	NA	-8	NA

Table S4. Descriptive circular statistics for *in vivo* bone strain orientations in the jugal of *Uromastyx*, sorted by bite location.

Experiment and side	**Exp 220 Right**			**Exp 220 Left**		**Exp 256 Right**		
Bite point	Front	WS	BS	WS	BS	Front	WS	BS
Number of Observations	53	123	102	8	5	25	62	25
Mean Vector (μ)	24.882°	31.5°	33.951°	12.012°	15.047°	32.143°	36.148°	30.123°
Length of Mean Vector (r)	0.925	0.842	0.595	0.736	0.982	0.061	0.591	0.604
Median	24.555°	31.669°	33.062°	16.555°	15.986°	41.158°	35.756°	33.923°
Concentration	6.95	3.498	1.49	1.486	13.596	0.123	1.473	1.523
Circular Variance	0.037	0.079	0.202	0.132	0.009	0.469	0.204	0.198
Circular Standard Deviation	11.309°	16.782°	29.18°	22.423°	5.502°	67.668°	29.374°	28.789°
Standard Error of Mean	1.552°	1.505°	3.012°	9.684°	3.507°	65.876°	3.898°	5.975°
95% Confidence Interval (-/+) for μ	21.84°	28.55°	28.047°	353.029°	8.172°	263°	28.505°	18.409°
	27.925°	34.45°	39.856°	30.996°	21.922°	161.286°	43.79°	41.837°
99% Confidence Interval (-/+) for μ	20.884°	27.623°	26.192°	347.066°	6.013°	222.433°	26.105°	14.73°
	28.881°	35.376°	41.711°	36.959°	24.081°	201.852°	46.191°	45.516°
Rayleigh Test (Z)	45.352	87.272	36.144	4.335	4.819	0.094	21.667	9.106
Rayleigh Test (p)	< 1E-12	< 1E-12	< 1E-12	0.009	0.002	0.912	3.89E-10	4.85E-05
Watson's U^2 Test (von Mises, U^2)	0.172	1.923	0.488	*****	*****	0.296	1.313	0.594
Watson's U^2 Test (p)	< 0.01	< 0.005	< 0.005	*****	*****	< 0.005	< 0.005	< 0.005
Circular-linear correlation (r)	0.226	0.308	0.293	0.63	0.792	0.156	0.314	0.235
Circular-linear correlation (P)	0.077	1.09E-05	2.00E-04	0.123	0.23	0.587	0.003	0.298

***** indicates that a result could not be calculated.

Table S4 (cont.).

Experiment and side	Exp 256 Left			Exp 257 Right			Exp 257 Left		
Bite point	Front	WS	BS	Front	WS	BS	Front	WS	BS
Number of Observations	28	25	65	30	11	5	30	5	11
Mean Vector (μ)	60.965°	55.245°	71.266°	178.516°	134.265°	151.687°	111.789°	167.294°	165.804°
Length of Mean Vector (r)	0.23	0.889	0.304	0.52	0.909	0.85	0.143	0.985	0.894
Median	64.473°	56.915°	69.357°	6.83°	136.95°	145.953°	117.15°	165.329°	170.327°
Concentration	0.473	4.803	0.639	1.214	4.31	1.795	0.289	16.583	3.726
Circular Variance	0.385	0.055	0.348	0.24	0.045	0.075	0.428	0.007	0.053
Circular Standard Deviation	49.12°	13.893°	44.192°	32.743°	12.511°	16.337°	56.501°	4.974°	13.578°
Standard Error of Mean	16.424°	2.773°	8.059°	6.582°	4.364°	10.372°	25.729°	3.17°	4.734°
95% Confidence Interval (-/+) for μ	28.768°	49.809°	55.467°	165.613°	125.71°	131.355°	61.349°	161.08°	156.524°
	93.162°	60.681°	87.065°	191.419°	142.82°	172.02°	162.228°	173.509°	175.084°
99% Confidence Interval (-/+) for μ	18.655°	48.102°	50.504°	161.56°	123.023°	124.968°	45.505°	159.128°	153.61°
	103.275°	62.388°	92.028°	195.472°	145.507°	178.407°	178.072°	175.461°	177.998°
Rayleigh Test (Z)	1.48	19.761	6.018	8.124	9.09	3.612	0.613	4.852	8.787
Rayleigh Test (p)	0.229	5.60E-09	0.002	1.81E-04	< 1E-12	0.018	0.545	0.002	< 1E-12
Watson's U^2 Test (von Mises, U^2)	0.323	0.249	0.685	0.32	0.195	*****	0.046	*****	0.276
Watson's U^2 Test (p)	< 0.005	< 0.005	< 0.005	< 0.005	< 0.005	*****	0.25 > p > 0.15	*****	< 0.005
Circular-linear correlation (r)	0.205	0.236	0.34	0.66	0.678	0.572	0.776	0.468	0.483
Circular-linear correlation (P)	0.351	0.293	7.37E-04	3.35E-06	0.019	0.506	6.97E-09	0.641	0.15

***** indicates that a result could not be calculated.

Table S5. Descriptive circular statistics for *in vivo* bone strain orientations in the jugal of *Uromastyx*, sorted by food type.

Experiment and side	**Exp 220 Right**			**Exp 220 Left**			**Exp 256 Right**	
Food type	Greens	Mazuri	Transducer	Greens	Mazuri	Transducer	Greens	Mazuri
Number of Observations	221	129	39	15	41	11	415	128
Mean Vector (μ)	33.827°	31.072°	22.43°	10.495°	179.525°	179.373°	27.406°	41.721°
Length of Mean Vector (r)	0.77	0.72	0.918	0.46	0.825	0.41	0.246	0.068
Median	32.65°	28.857°	20.771°	179.393°	179.159°	15.461°	32.033°	42.64°
Concentration	2.54	2.138	6.417	0.905	3.198	0.697	0.507	0.135
Circular Variance	0.115	0.14	0.041	0.27	0.088	0.295	0.377	0.466
Circular Standard Deviation	20.712°	23.209°	11.814°	35.705°	17.792°	38.241°	48.009°	66.513°
Standard Error of Mean	1.378°	2.033°	1.89°	11.463°	2.755°	16.151°	3.987°	26.486°
95% Confidence Interval (-/+) for μ	31.126°	27.087°	18.725°	348.023°	174.124°	147.71°	19.59°	349.797°
	36.529°	35.056°	26.134°	32.967°	184.926°	211.036°	35.221°	93.644°
99% Confidence Interval (-/+) for μ	30.278°	25.835°	17.562°	340.964°	172.427°	137.764°	17.135°	333.487°
	37.377°	36.308°	27.298°	40.025°	186.623°	220.981°	37.676°	109.955°
Rayleigh Test (Z)	131.033	66.917	32.901	3.173	27.879	1.852	25.026	0.584
Rayleigh Test (p)	< 1E-12	< 1E-12	< 1E-12	0.039	3.62E-12	0.158	1.35E-11	0.558
Watson's U^2 Test (von Mises, U^2)	2.473	0.635	0.176	0.145	0.051	0.14	6.471	1.602
Watson's U^2 Test (p)	< 0.005	< 0.005	< 0.01	< 0.005	0.5 > p > 0.25	< 0.005	< 0.005	< 0.005
Circular-linear correlation (r)	0.331	0.19	0.342	0.593	0.398	0.672	0.191	0.18
Circular-linear correlation (P)	3.60E-11	0.011	0.015	0.012	0.002	0.02	2.88E-07	0.018

Table S5 (cont.).

Experiment and side	Exp 256 Left		Exp 257 Right		Exp 257 Left	
Food type	Greens	Mazuri	Greens	Mazuri	Greens	Mazuri
Number of Observations	421	208	275	64	275	64
Mean Vector (μ)	60.51°	160.019°	157.109°	112.807°	160.894°	163.883°
Length of Mean Vector (r)	0.372	0.252	0.585	0.612	0.509	0.41
Median	60.371°	154.669°	149.356°	106.376°	162.535°	172.031°
Concentration	0.803	0.52	1.45	1.56	1.177	0.898
Circular Variance	0.314	0.374	0.207	0.194	0.246	0.295
Circular Standard Deviation	40.263°	47.587°	29.651°	28.378°	33.312°	38.264°
Standard Error of Mean	2.554°	5.49°	1.875°	3.664°	2.233°	5.902°
95% Confidence Interval (-/+) for μ	55.503°	149.256°	153.433°	105.624°	156.517°	152.312°
	65.516°	170.781°	160.784°	119.991°	165.271°	175.454°
99% Confidence Interval (-/+) for μ	53.931°	145.875°	152.278°	103.368°	155.142°	148.677°
	67.089°	174.162°	161.939°	122.247°	166.645°	179.089°
Rayleigh Test (Z)	58.402	13.175	94.207	23.991	71.142	10.749
Rayleigh Test (p)	< 1E-12	1.90E-06	< 1E-12	3.81E-11	< 1E-12	2.15E-05
Watson's U^2 Test (von Mises, U^2)	5.533	2.304	2.256	0.298	0.752	0.732
Watson's U^2 Test (p)	< 0.005	< 0.005	< 0.005	< 0.005	< 0.005	< 0.005
Circular-linear correlation (r)	0.453	0.329	0.501	0.621	0.536	0.41
Circular-linear correlation (P)	< 1E-12	2.14E-10	< 1E-12	1.67E-11	< 1E-12	3.19E-05

Table S6. Descriptive circular statistics for *in vivo* bone strain orientations in the jugal of *Uromastyx*, sorted by feeding behavior.

Experiment and side	**Exp 220 Right**							
Behavior	Flick	Capture	Manipulation	Crush	Chew	Swallow	Lick	Tear
Number of Observations	4	4	128	5	175	11	46	4
Mean Vector (μ)	53.414°	52.609°	31.104°	22.069°	31.816°	40.633°	28.838°	26.211°
Length of Mean Vector (r)	0.981	0.995	0.751	0.95	0.776	0.73	0.695	0.956
Median	50.399°	51.488°	29.508°	20.433°	31.653°	35.476°	26.105°	30.056°
Concentration	10.699	37.38	2.369	5.009	2.599	1.643	1.977	4.658
Circular Variance	0.009	0.003	0.125	0.025	0.112	0.135	0.152	0.022
Circular Standard Deviation	5.571°	2.96°	21.689°	9.221°	20.4°	22.746°	24.426°	8.556°
Standard Error of Mean	4.421°	2.349°	1.898°	5.875°	1.525°	7.889°	3.603°	6.787°
95% Confidence Interval (-/+) for μ	44.747°	48.004°	27.382°	10.552°	28.826°	25.167°	21.776°	12.906°
	62.08°	57.215°	34.826°	33.586°	34.805°	56.099°	35.9°	39.516°
99% Confidence Interval (-/+) for μ	42.025°	46.558°	26.213°	6.934°	27.887°	20.308°	19.557°	8.727°
	64.802°	58.661°	35.995°	37.204°	35.744°	60.958°	38.119°	43.695°
Rayleigh Test (Z)	3.852	3.958	72.159	4.508	105.395	5.856	22.235	3.659
Rayleigh Test (p)	0.009	0.008	**< 1E-12**	0.004	< 1E-12	0.001	1.99E-10	0.014
Watson's U^2 Test (von Mises, U^2)	*****	*****	0.996	*****	1.691	0.068	0.325	*****
Watson's U^2 Test (p)	*****	*****	< 0.005	*****	< 0.005	0.25 > p > 0.15	< 0.005	*****
Circular-linear correlation (r)	0.997	0.848	0.315	0.484	0.284	0.254	0.238	0.865
Circular-linear correlation (P)	0.057	0.405	4.06E-06	0.62	9.52E-07	0.596	0.088	0.38

***** indicates that a result could not be calculated.

Table S6 (cont.).

Experiment and side	**Exp 220 Left**					
Behavior	Flick	Capture	Manipulation	Chew	Swallow	Lick
Number of Observations	4	3	17	10	4	19
Mean Vector (μ)	171.345°	165.614°	13.579°	5.193°	169.99°	3.116°
Length of Mean Vector (r)	0.99	1	0.648	0.564	0.988	0.791
Median	172.091°	165.835°	17.549°	92.87°	170.041°	0.187°
Concentration	19.964	311.081	1.721	1.223	17.253	2.761
Circular Variance	0.005	2.14E-04	0.176	0.218	0.006	0.104
Circular Standard Deviation	4.061°	0.839°	26.697°	30.672°	4.371°	19.597°
Standard Error of Mean	3.222°	0.938°	6.58°	10.909°	3.469°	4.446°
95% Confidence Interval (-/+) for μ	165.029°	163.775°	0.679°	343.806°	163.19°	354.4°
	177.661°	167.453°	26.479°	26.58°	176.79°	11.832°
99% Confidence Interval (-/+) for μ	163.045°	163.198°	356.627°	337.088°	161.054°	351.662°
	179.646°	168.031°	30.531°	33.298°	178.926°	14.57°
Rayleigh Test (Z)	3.92	2.997	7.133	3.178	3.908	11.899
Rayleigh Test (p)	0.008	0.034	3.90E-04	0.037	0.008	8.90E-07
Watson's U^2 Test (von Mises, U^2)	*****	*****	0.207	0.038	*****	0.265
Watson's U^2 Test (p)	*****	*****	< 0.005	0.5 > p > 0.25	*****	< 0.005
Circular-linear correlation (r)	0.999	1	0.356	0.92	0.913	0.291
Circular-linear correlation (P)	0.027	1	0.169	1.66E-04	0.301	0.257

***** indicates that a result could not be calculated.

Table S6 (cont.).

Experiment and side	**Exp 256 Right**						
Behavior	Flick	Capture	Manipulation	Crush	Chew	Swallow	Lick
Number of Observations	9	48	136	23	214	91	9
Mean Vector (μ)	131.394°	157.209°	30.556°	35.452°	33.888°	125.265°	126.08°
Length of Mean Vector (r)	0.782	0.119	0.634	0.813	0.412	0.725	0.996
Median	130.223°	152.891°	32.871°	37.064°	33.928°	124.955°	126.226°
Concentration	1.842	0.239	1.654	3.025	0.904	2.168	85.147
Circular Variance	0.109	0.441	0.183	0.094	0.294	0.138	0.002
Circular Standard Deviation	20.114°	59.125°	27.368°	18.453°	38.146°	22.997°	2.591°
Standard Error of Mean	7.959°	24.51°	2.399°	3.81°	3.208°	2.396°	1.037°
95% Confidence Interval (-/+) for μ	115.79°	109.161°	25.852°	27.983°	27.598°	120.568°	124.047°
	146.997°	205.258°	35.26°	42.921°	40.177°	129.962°	128.113°
99% Confidence Interval (-/+) for μ	110.889°	94.068°	24.375°	25.637°	25.622°	119.092°	123.408°
	151.898°	220.351°	36.737°	45.268°	42.153°	131.437°	128.751°
Rayleigh Test (Z)	5.497	0.678	54.599	15.19	36.34	47.772	8.927
Rayleigh Test (p)	0.002	0.51	< 1E-12	1.05E-07	< 1E-12	< 1E-12	< 1E-12
Watson's U^2 Test (von Mises, U^2)	*****	0.415	3.504	0.631	3.906	1.846	*****
Watson's U^2 Test (p)	*****	< 0.005	< 0.005	< 0.005	< 0.005	< 0.005	*****
Circular-linear correlation (r)	0.551	0.381	0.303	0.484	0.224	0.448	0.491
Circular-linear correlation (P)	0.152	0.001	4.79E-06	0.008	2.39E-05	1.63E-08	0.229

***** indicates that a result could not be calculated.

Table S6 (cont.).

Experiment and side	Exp 256 Left						
Behavior	Flick	Capture	Manipulation	Crush	Chew	Swallow	Lick
Number of Observations	13	56	143	36	230	120	18
Mean Vector (μ)	157.66°	167.845°	60.217°	59.745°	60.54°	155.251°	152.424°
Length of Mean Vector (r)	0.394	0.11	0.606	0.735	0.403	0.587	0.993
Median	154.058°	171.176°	60.549°	60.273°	60.6°	154.282°	152.741°
Concentration	0.678	0.222	1.534	2.242	0.88	1.456	72.996
Circular Variance	0.303	0.445	0.197	0.133	0.299	0.207	0.003
Circular Standard Deviation	39.099°	60.14°	28.668°	22.496°	38.637°	29.583°	3.365°
Standard Error of Mean	15.377°	24.441°	2.484°	3.72°	3.174°	2.829°	0.793°
95% Confidence Interval (-/+) for μ	127.514°	119.931°	55.347°	52.452°	54.319°	149.704°	150.869°
	187.806°	215.759°	65.088°	67.038°	66.762°	160.798°	153.979°
99% Confidence Interval (-/+) for μ	118.045°	104.88°	53.817°	50.161°	52.364°	147.962°	150.381°
	197.275°	230.81°	66.618°	69.329°	68.717°	162.54°	154.467°
Rayleigh Test (Z)	2.018	0.683	52.532	19.432	37.305	41.312	17.753
Rayleigh Test (p)	0.133	0.505	< 1E-12	2.63E-09	< 1E-12	< 1E-12	5.03E-08
Watson's U^2 Test (von Mises, U^2)	0.256	0.583	1.976	0.394	3.013	2.215	0.316
Watson's U^2 Test (p)	< 0.005	< 0.005	< 0.005	< 0.005	< 0.005	< 0.005	< 0.005
Circular-linear correlation (r)	0.356	0.282	0.322	0.223	0.444	0.26	0.708
Circular-linear correlation (P)	0.279	0.015	4.66E-07	0.193	< 1E-12	3.61E-04	2.60E-04

***** indicates that a result could not be calculated.

Table S6 (cont.).

Experiment and side	**Exp 257 Right**						
Behavior	Flick	Capture	Manipulation	Crush	Chew	Swallow	Lick
Number of Observations	10	51	103	4	108	34	26
Mean Vector (μ)	172.37°	161.264°	159.361°	137.73°	152.589°	103.141°	107.996°
Length of Mean Vector (r)	0.418	0.483	0.706	0.996	0.613	0.666	0.637
Median	82.71°	150.467°	150.672°	137.04°	147.877°	104.251°	104.275°
Concentration	0.703	1.102	2.042	45.349	1.561	1.812	1.671
Circular Variance	0.291	0.258	0.147	0.002	0.194	0.167	0.181
Circular Standard Deviation	37.82°	34.538°	23.917°	2.687°	28.362°	25.842°	27.193°
Standard Error of Mean	16.701°	5.496°	2.351°	2.132°	2.819°	4.474°	5.444°
95% Confidence Interval (-/+) for μ	139.629°	150.49°	154.751°	133.551°	147.063°	94.371°	97.324°
	205.11°	172.037°	163.97°	141.909°	158.114°	111.911°	118.667°
99% Confidence Interval (-/+) for μ	129.345°	147.105°	153.304°	132.238°	145.328°	91.616°	93.972°
	215.395°	175.422°	165.418°	143.221°	159.85°	114.666°	122.019°
Rayleigh Test (Z)	1.75	11.921	51.302	3.965	40.529	15.069	10.56
Rayleigh Test (p)	0.176	6.65E-06	< 1E-12	0.008	< 1E-12	7.24E-08	8.30E-06
Watson's U^2 Test (von Mises, U^2)	0.16	0.434	1.316	*****	1.045	0.185	0.403
Watson's U^2 Test (p)	< 0.005	< 0.005	< 0.005	*****	< 0.005	< 0.005	< 0.005
Circular-linear correlation (r)	0.705	0.634	0.365	0.748	0.457	0.511	0.941
Circular-linear correlation (P)	0.022	1.31E-09	1.56E-06	0.531	2.23E-10	2.55E-04	< 1E-12

***** indicates that a result could not be calculated.

Table S6 (cont.).

Experiment and side	Exp 257 Left						
Behavior	Flick	Capture	Manipulation	Crush	Chew	Swallow	Lick
Number of Observations	10	51	103	4	108	34	26
Mean Vector (μ)	99.344°	125.68°	167.768°	170.866°	160.342°	104.288°	178.06°
Length of Mean Vector (r)	0.324	0.435	0.857	0.997	0.545	0.088	0.549
Median	115.291°	120.043°	165.819°	170.075°	161.472°	106.751°	178.258°
Concentration	0.395	0.964	3.803	62.448	1.302	0.176	1.315
Circular Variance	0.338	0.283	0.072	0.002	0.228	0.456	0.226
Circular Standard Deviation	42.982°	36.98°	15.927°	2.288°	31.571°	63.198°	31.396°
Standard Error of Mean	25.317°	6.196°	1.564°	1.815°	3.273°	39.514°	6.616°
95% Confidence Interval (-/+) for μ	49.713°	113.535°	164.702°	167.307°	153.926°	26.825°	165.09°
	148.976°	137.826°	170.833°	174.425°	166.759°	181.75°	191.029°
99% Confidence Interval (-/+) for μ	34.123°	109.719°	163.739°	166.189°	151.911°	2.493°	161.016°
	164.566°	141.641°	171.796°	175.543°	168.774°	206.083°	195.103°
Rayleigh Test (Z)	1.053	9.637	75.614	3.975	32.06	0.262	7.823
Rayleigh Test (p)	0.358	6.53E-05	< 1E-12	0.007	< 1E-12	0.772	2.36E-04
Watson's U^2 Test (von Mises, U^2)	0.064	0.167	0.161	*****	0.303	0.168	0.531
Watson's U^2 Test (p)	0.1 > p > 0.05	< 0.005	< 0.01	*****	< 0.005	< 0.005	< 0.005
Circular-linear correlation (r)	0.619	0.585	0.416	1	0.523	0.257	0.304
Circular-linear correlation (P)	0.059	3.62E-08	2.52E-08	0.006	< 1E-12	0.128	0.119

***** indicates that a result could not be calculated.

Table S7. Results of Mardia-Watson-Wheeler tests to determine whether ε1 angle distributions are identical within gage sites, sorted by bite location.

Experiment and side	W	p
Exp 220 Right		
Front E1 angle & WS E1 angle	17.431	1.64E-04
Front E1 angle & BS E1 angle	26.519	1.74E-06
WS E1 angle & BS E1 angle	25.527	2.86E-06
Exp 220 Left		
WS E1 angle & BS E1 angle	*****	*****
Exp 256 Right		
Front E1 angle & WS E1 angle	7.408	0.025
Front E1 angle & BS E1 angle	12.697	0.002
WS E1 angle & BS E1 angle	6.851	0.033
Exp 256 Left		
Front E1 angle & WS E1 angle	20.159	4.19E-05
Front E1 angle & BS E1 angle	1.895	0.388
WS E1 angle & BS E1 angle	34.748	2.85E-08
Exp 257 Right		
Front E1 angle & WS E1 angle	14.208	8.22E-04
Front E1 angle & BS E1 angle	*****	*****
WS E1 angle & BS E1 angle	*****	*****
Exp 257 Left		
Front E1 angle & WS E1 angle	*****	*****
Front E1 angle & BS E1 angle	16.45	2.68E-04
WS E1 angle & BS E1 angle	*****	*****

***** indicates that a result could not be calculated.

Table S8. Results of Mardia-Watson-Wheeler tests to determine whether ε1 angle distributions are identical within gage sites, sorted by food type.

Experiment and side	W	p
Exp 220 Right		
Greens E1 angle & Mazuri E1 angle	29.314	4.31E-07
Greens E1 angle & Transducer E1 angle	40.127	1.93E-09
Mazuri E1 angle & Transducer E1 angle	11.366	0.003
Exp 220 Left		
Greens E1 angle & Mazuri E1 angle	3.882	0.144
Greens E1 angle & Transducer E1 angle	1.258	0.533
Mazuri E1 angle & Transducer E1 angle	17.01	2.02E-04
Exp 256 Right		
Greens E1 angle & Mazuri E1 angle	48.239	3.35E-11
Exp 256 Left		
Greens E1 angle & Mazuri E1 angle	60.079	< 1E-12
Exp 257 Right		
Greens E1 angle & Mazuri E1 angle	103.863	< 1E-12
Exp 257 Left		
Greens E1 angle & Mazuri E1 angle	16.444	2.69E-04

Table S9. Results of Mardia-Watson-Wheeler tests to determine whether ε1 angle distributions are identical within gage sites, sorted by feeding behavior.

Experiment and side	W	p
Exp 220 Right		
Flick E1 angle & Capture E1 angle	*****	*****
Flick E1 angle & Manip. E1 angle	*****	*****
Flick E1 angle & Crush E1 angle	*****	*****
Flick E1 angle & Chew E1 angle	*****	*****
Flick E1 angle & Swallow E1 angle	*****	*****
Flick E1 angle & Lick E1 angle	*****	*****
Flick E1 angle & Tear E1 angle	*****	*****
Capture E1 angle & Manip. E1 angle	*****	*****
Capture E1 angle & Crush E1 angle	*****	*****
Capture E1 angle & Chew E1 angle	*****	*****
Capture E1 angle & Swallow E1 angle	*****	*****
Capture E1 angle & Lick E1 angle	*****	*****
Capture E1 angle & Tear E1 angle	*****	*****
Manip. E1 angle & Crush E1 angle	*****	*****
Manip. E1 angle & Chew E1 angle	9.152	0.01
Manip. E1 angle & Swallow E1 angle	5.904	0.052
Manip. E1 angle & Lick E1 angle	4.8	0.091
Manip. E1 angle & Tear E1 angle	*****	*****
Crush E1 angle & Chew E1 angle	*****	*****
Crush E1 angle & Swallow E1 angle	*****	*****
Crush E1 angle & Lick E1 angle	*****	*****
Crush E1 angle & Tear E1 angle	*****	*****
Chew E1 angle & Swallow E1 angle	4.244	0.12
Chew E1 angle & Lick E1 angle	14.349	7.66E-04
Chew E1 angle & Tear E1 angle	*****	*****
Swallow E1 angle & Lick E1 angle	5.67	0.059
Swallow E1 angle & Tear E1 angle	*****	*****
Lick E1 angle & Tear E1 angle	*****	*****
Exp 220 Left		
Flick E1 angle & Capture E1 angle	*****	*****
Flick E1 angle & Manip. E1 angle	*****	*****
Flick E1 angle & Chew E1 angle	*****	*****
Flick E1 angle & Swallow E1 angle	*****	*****
Flick E1 angle & Lick E1 angle	*****	*****
Capture E1 angle & Manip. E1 angle	*****	*****
Capture E1 angle & Chew E1 angle	*****	*****
Capture E1 angle & Swallow E1 angle	*****	*****
Capture E1 angle & Lick E1 angle	*****	*****

Table S9 (cont.).

Experiment and side	W	p
Exp 220 Left		
Manip.E1 andlg & Chew E1 angle	6.312	0.043
Manip. E1 angle & Swallow E1 angle	*****	*****
Manip. E1 angle & Lick E1 angle	19.123	7.04E-05
Chew E1 angle & Swallow E1 angle	*****	*****
Chew E1 angle & Lick E1 angle	6.705	0.035
Swallow E1 angle & Lick E1 angle	*****	*****
Exp 256 Right		
Flick E1 angle & Capture E1 angle	*****	*****
Flick E1 angle & Manip. E1 angle	*****	*****
Flick E1 angle & Crush E1 angle	*****	*****
Flick E1 angle & Chew E1 angle	*****	*****
Flick E1 angle & Swallow E1 angle	*****	*****
Flick E1 angle & Lick E1 angle	*****	*****
Capture E1 angle & Manip. E1 angle	32.137	1.05E-07
Capture E1 angle & Crush E1 angle	19.108	7.09E-05
Capture E1 angle & Chew E1 angle	16.629	2.45E-04
Capture E1 angle & Swallow E1 angle	16.796	2.25E-04
Capture E1 angle & Lick E1 angle	*****	*****
Manip. E1 angle & Crush E1 angle	15.282	4.80E-04
Manip. E1 angle & Chew E1 angle	22.608	1.23E-05
Manip. E1 angle & Swallow E1 angle	115.881	< 1E-12
Manip. E1 angle & Lick E1 angle	*****	*****
Crush E1 angle & Chew E1 angle	7.191	0.027
Crush E1 angle & Swallow E1 angle	35.896	1.60E-08
Crush E1 angle & Lick E1 angle	*****	*****
Chew E1 angle & Swallow E1 angle	81.005	< 1E-12
Chew E1 angle & Lick E1 angle	*****	*****
Swallow E1 angle & Lick E1 angle	*****	*****
Exp 256 Left		
Flick E1 angle & Capture E1 angle	1.401	0.496
Flick E1 angle & Manip. E1 angle	11.843	0.003
Flick E1 angle & Crush E1 angle	10.349	0.006
Flick E1 angle & Chew E1 angle	9.432	0.009
Flick E1 angle & Swallow E1 angle	1.135	0.567
Flick E1 angle & Lick E1 angle	12.277	0.002
Capture E1 angle & Manip. E1 angle	16.284	2.91E-04
Capture E1 angle & Crush E1 angle	11.449	0.003
Capture E1 angle & Chew E1 angle	10.527	0.005
Capture E1 angle & Swallow E1 angle	11.16	0.004
Capture E1 angle & Lick E1 angle	24.289	5.32E-06
Manip. E1 angle & Crush E1 angle	0.183	0.913

Table S9 (cont.).

Experiment and side	W	p
Exp 256 Left		
Manip. E1 angle & Chew E1 angle	2.259	0.323
Manip. E1 angle & Swallow E1 angle	83.745	< 1E-12
Manip. E1 angle & Lick E1 angle	37.653	6.67E-09
Crush E1 angle & Chew E1 angle	1.482	0.477
Crush E1 angle & Swallow E1 angle	45.889	1.08E-10
Crush E1 angle & Lick E1 angle	36.973	9.36E-09
Chew E1 angle & Swallow E1 angle	76.419	< 1E-12
Chew E1 angle & Lick E1 angle	36.954	9.45E-09
Swallow E1 angle & Lick E1 angle	17.655	1.47E-04
Exp 257 Right		
Flick E1 angle & Capture E1 angle	1.935	0.38
Flick E1 angle & Manip. E1 angle	15.056	5.38E-04
Flick E1 angle & Crush E1 angle	*****	*****
Flick E1 angle & Chew E1 angle	9.388	0.009
Flick E1 angle & Swallow E1 angle	20.556	3.44E-05
Flick E1 angle & Lick E1 angle	16.106	3.18E-04
Capture E1 angle & Manip. E1 angle	12.919	0.002
Capture E1 angle & Crush E1 angle	*****	*****
Capture E1 angle & Chew E1 angle	6.261	0.044
Capture E1 angle & Swallow E1 angle	49.974	1.41E-11
Capture E1 angle & Lick E1 angle	35.917	1.59E-08
Manip. E1 angle & Crush E1 angle	*****	*****
Manip. E1 angle & Chew E1 angle	2.309	0.315
Manip. E1 angle & Swallow E1 angle	64.764	< 1E-12
Manip. E1 angle & Lick E1 angle	54.102	1.79E-12
Crush E1 angle & Chew E1 angle	*****	*****
Crush E1 angle & Swallow E1 angle	*****	*****
Crush E1 angle & Lick E1 angle	*****	*****
Chew E1 angle & Swallow E1 angle	55.045	1.11E-12
Chew E1 angle & Lick E1 angle	45.507	1.31E-10
Swallow E1 angle & Lick E1 angle	3.159	0.206
Exp 257 Left		
Flick E1 angle & Capture E1 angle	2.069	0.355
Flick E1 angle & Manip. E1 angle	14.3	7.85E-04
Flick E1 angle & Crush E1 angle	*****	*****
Flick E1 angle & Chew E1 angle	8.376	0.015
Flick E1 angle & Swallow E1 angle	0.177	0.915
Flick E1 angle & Lick E1 angle	8.048	0.018
Capture E1 angle & Manip. E1 angle	41.564	9.43E-10
Capture E1 angle & Crush E1 angle	*****	*****
Capture E1 angle & Chew E1 angle	16.571	2.52E-04

Table S9 (cont.).

Experiment and side	W	p
Exp 257 Left		
Capture E1 angle & Swallow E1 angle	9.991	0.007
Capture E1 angle & Lick E1 angle	19.452	5.97E-05
Manip. E1 angle & Crush E1 angle	*****	*****
Manip. E1 angle & Chew E1 angle	14.525	7.01E-04
Manip. E1 angle & Swallow E1 angle	32.287	9.75E-08
Manip. E1 angle & Lick E1 angle	21.335	2.33E-05
Crush E1 angle & Chew E1 angle	*****	*****
Crush E1 angle & Swallow E1 angle	*****	*****
Crush E1 angle & Lick E1 angle	*****	*****
Chew E1 angle & Swallow E1 angle	23.217	9.09E-06
Chew E1 angle & Lick E1 angle	27.269	1.20E-06
Swallow E1 angle & Lick E1 angle	12.665	0.002

***** indicates that a result could not be calculated.

Table S10. ANOVA testing for differences in ε1 and ε2 and shear strain magnitudes and principal strain ratios due to food type and behavior. All individuals were included in right gage analyses; only *Uro1* and *Uro7* were included in left gage analyses. Behaviors analyzed include: captures (left only), manipulations, chews, swallows and licks.

E1

RIGHT GAGE				LEFT GAGE			
Source	*d.f.*	*F*	*P*	*Source*	*d.f.*	*F*	*P*
Food	1,1029	**31.9679**	**<0.0001**	Food	1,875.1	0.8029	0.3705
Behavior	3,1030	**27.6119**	**<0.0001**	Behavior	4,875	**34.8462**	**<0.0001**
Food*Behavior	3,1030	2.4535	0.0619	Food*Behavior	4,875	**3.4904**	**0.0077**

E2

RIGHT GAGE				LEFT GAGE			
Source	*d.f.*	*F*	*P*	*Source*	*d.f.*	*F*	*P*
Food	1,1025	2.1888	0.1339	Food	1,876.1	0.8057	0.3696
Behavior	3,1026	**87.5332**	**<0.0001**	Behavior	4,876.1	**56.7883**	**<0.0001**
Food*Behavior	3,1026	**2.7081**	**0.0441**	Food*Behavior	4,876	**9.6662**	**<0.0001**

Shear strain

RIGHT GAGE				LEFT GAGE			
Source	*d.f.*	*F*	*P*	*Source*	*d.f.*	*F*	*P*
Food	1,1032	**19.8208**	**<0.0001**	Food	1,879	0.4188	0.5177
Behavior	3,1033	**72.9793**	**<0.0001**	Behavior	4,879	**59.4123**	**<0.0001**
Food*Behavior	3,1032	1.9731	0.1163	Food*Behavior	4,879	**8.2731**	**<0.0001**

|ε1 / ε2|

RIGHT GAGE				LEFT GAGE			
Source	*d.f.*	*F*	*P*	*Source*	*d.f.*	*F*	*P*
Food	1,1032	0.1069	0.7438	Food	1,879.7	**6.2823**	**0.0124**
Behavior	3,1033	**82.1776**	**<0.0001**	Behavior	4,879.4	**6.5309**	**<0.0001**
Food*Behavior	3,1032	**2.9200**	**0.0331**	Food*Behavior	4,879.1	**2.9960**	**0.0180**

Table S11. ANOVA testing for differences in ε1 and ε2 and shear strain magnitudes due to bite location.

E1

RIGHT GAGE				LEFT GAGE			
Source	*d.f.*	*F*	*P*	*Source*	*d.f.*	*F*	*P*
Side	2,389.1	**25.6374**	**<0.0001**	Side	2,168.1	**9.4276**	**<0.0001**

E2

RIGHT GAGE				LEFT GAGE			
Source	*d.f.*	*F*	*P*	*Source*	*d.f.*	*F*	*P*
Side	2,395	**22.2243**	**<0.0001**	Side	2,170.3	**11.0651**	**<0.0001**

Shear strain

RIGHT GAGE				LEFT GAGE			
Source	*d.f.*	*F*	*P*	*Source*	*d.f.*	*F*	*P*
Side	2,400.4	**28.6351**	**<0.0001**	Side	2,170.3	**10.9370**	**<0.0001**

|ε1 / ε2|

RIGHT GAGE				LEFT GAGE			
Source	*d.f.*	*F*	*P*	*Source*	*d.f.*	*F*	*P*
Side	2,400	**5.5684**	**0.0041**	Side	2,166.2	**7.0780**	**0.0011**

Table S12. Two-way ANOVA testing for differences in ε1 orientation due to food type and behavior. All individuals were included in right gage analyses; *Uro1* and *Uro7* were included in left gage analyses. As individual variation could not be included as a random effect, individuals were tested separately.

***Uro5* (Experiment 220)**

RIGHT GAGE			
Source	*d.f.*	*F*	*P*
Food	1	1.4018	0.2373
Behavior	3	1.7444	0.1579
Food*Behavior	3	1.7618	0.1544

***Uro1* (Experiment 256)**

RIGHT GAGE				LEFT GAGE			
Source	*d.f.*	X^2	*P*	*Source*	*d.f.*	X^2	*P*
Food	2	**33.4681**	**<0.0001**	Food	2	**33.4681**	**<0.0001**
Behavior	6	**265.8169**	**<0.0001**	Behavior	6	**265.8169**	**<0.0001**
Food*Behavior	3	-22.7757	1	Food*Behavior	3	-22.7757	1

***Uro7* (Experiment 257)**

RIGHT GAGE				LEFT GAGE			
Source	*d.f.*	X^2	*P*	*Source*	*d.f.*	X^2	*P*
Food	2	**84.7385**	**<0.0001**	Food	2	3.4870	0.1749
Behavior	6	**132.4011**	**<0.0001**	Behavior	8	**115.6787**	**<0.0001**
Food*Behavior	3	-56.1329	1	Food*Behavior	4	4.7968	0.8910

Table S13. ANOVA testing for differences in ε1 orientation due to bite location. All individuals were included in right gage analyses; *Uro1* and *Uro7* were included in left gage analyses. As individual variation could not be included as a random effect, individuals were tested separately.

***Uro5* (Experiment 220)**

RIGHT GAGE			
Source	*d.f.*	*F*	*P*
Food	2	**3.5008**	**0.0315**

***Uro1* (Experiment 256)**

RIGHT GAGE				LEFT GAGE			
Source	*d.f.*	*F*	*P*	*Source*	*d.f.*	*F*	*P*
Food	2	0.3009	0.7407	Food	2	1.9170	0.1517

***Uro7* (Experiment 257)**

RIGHT GAGE				LEFT GAGE			
Source	*d.f.*	*F*	*P*	*Source*	*d.f.*	*F*	*P*
Food	2	**12.3231**	**<0.0001**	Food	2	**5.7552**	**0.0061**